Impact of Atmospheric Intraseasonal Variability in the Indian Ocean: Low-Frequency Rectification in Equatorial Surface Current and Transport

WEIQING HAN

Program in Atmospheric and Oceanic Sciences, University of Colorado, Boulder, Colorado

PETER WEBSTER

School of Earth and Atmospheric Sciences, Georgia Institute of Technology, Atlanta, Georgia

ROGER LUKAS AND PETER HACKER

School of Ocean and Earth Science and Technology, University of Hawaii at Manoa, Honolulu, Hawaii

AIXUE HU

National Center for Atmospheric Research, Boulder, Colorado

(Manuscript received 27 November 2002, in final form 6 January 2004)

ABSTRACT

An ocean general circulation model (OGCM) is used to investigate the low-frequency (period longer than 90 days) rectification of atmospheric intraseasonal variability (10–90-day periods) in zonal surface current and transport of the equatorial Indian Ocean. A hierarchy of OGCM solutions is found in an actual tropical Indian Ocean basin for the period of 1988–2001. To help to identify and isolate nonlinear processes, a linear continuously stratified model and a $4\frac{1}{2}$-layer intermediate ocean model are also used. Results from the OGCM solutions suggest that intraseasonal atmospheric forcing acts to weaken the equatorial seasonal surface currents. Amplitudes of the spring and autumn eastward surface jets, the Wyrtki jets (WJ), and the westward surface current during January–March are reduced by as much as 15–25 cm s^{-1} by intraseasonal atmospheric forcing, and strengths of the rectification exhibit a significant interannual variability. Important processes that cause the low-frequency rectification are asymmetric response of mixed layer depth to easterly and westerly winds, entrainment, and upwelling of momentum. During spring and autumn, the westerly (easterly) phase of an intraseasonal event enhances (weakens or even reverses) the seasonal westerly winds, increases (decreases) equatorial convergence and entrainment, and thus deepens (thins) the mixed layer. A net, westward current is generated over an event mean because easterly wind acts on a thinner surface mixed layer whereas westerly wind acts on a thicker one. In contrast, during January–March when the seasonal winds are equatorial easterlies, surface currents are westward and equatorial undercurrents (EUC) develop. The rectified surface currents are eastward, which reduces the westward surface flow. This eastward rectification results largely from the vertical advection and entrainment of the EUC. The seasonal-to-interannual variability of the rectified surface flow is determined primarily from the seasonal cycle and interannual variability of the background state. Seasonal-to-interannual variability of the intraseasonal wind forcing also contributes. The rectified low-frequency zonal volume (heat) transports integrated over the entire water column along the Indian Ocean equator are persistently eastward with an amplitude of 0–15×10^6 m^3 s^{-1} (0–1.2 pW). This is because westerly winds generate equatorial downwelling, advecting the surface eastward momentum downward and giving an eastward subsurface current. Easterly winds cause equatorial upwelling and produce an eastward pressure gradient force that drives an eastward subsurface current. This eastward subsurface current is advected upward by upwelling. The mean effect over an intraseasonal event at the equator is to increase the eastward transport in the water column. In the layers above the thermocline, the rectified zonal volume (heat) transports are in the same direction as the rectified surface currents. Results from this paper may have important implications for understanding climate variability because modification of WJ strength and transports can affect the SST and heat storage in the equatorial Indian Ocean warm pool.

1. Introduction

a. Background

It was not until recent years that rectification of relatively high frequency intraseasonal atmospheric forc-

Corresponding author address: Dr. Weiqing Han, PAOS, University of Colorado, Campus Box 311, Boulder, CO 80309-0311.
E-mail: weiqing.han@colorado.edu

ing into seasonal-to-interannual oceanic variability has been quantitatively examined using numerical models (Kessler and Kleeman 2000; Waliser et al. 2003). Results from the two existing studies for the rectified zonal surface currents in the equatorial Pacific Ocean are opposite in sign, although they obtained similar rectified SST patterns.

Using the Gent and Cane (1989) sigma-coordinate ocean model, Kessler and Kleeman (2000) examined the rectification of the Madden–Julian oscillation (MJO) into the ENSO cycle in the tropical Pacific Ocean. Vertically, eight sigma levels plus a surface mixed layer were chosen to represent approximately the upper 400 m of the ocean. Two parallel runs were performed: one forced with climatological annual cycle of wind stress and the other with climatological winds plus idealized intraseasonal anomalies meant to correspond to MJO winds. Their results suggested that intraseasonal winds can produce a 15–20 cm s^{-1} eastward surface current at the equator that rectifies into the ENSO cycle. The theoretical basis provided by the authors was the argument made by Robinson (1966; see also Gill 1975), who showed that the first-order effect of nonlinearity of the ocean on an equatorial zonal current is to increase the eastward transport, whether the sign of the wind is eastward or westward. Easterly winds directly force a westward surface current. Meanwhile they also cause Ekman divergence that advects the westward momentum away from the equator, resulting in an eastward advective contribution at the equator. On the other hand, westerly winds force an eastward surface current and at the same time produce equatorial Ekman convergence that advects the momentum downward, increasing the eastward transport.

Using the same model but with 14 sigma levels in the Indo–Pacific basin, Waliser et al. (2003) obtained a westward, rather than eastward, rectified current in the equatorial Pacific, which is opposite in sign to that of Kessler and Kleeman (2000). However, rectified western Pacific cooling occurred in both simulations. Two parallel experiments similar to those of Kessler and Kleeman (2000) were performed except that realistic winter MJO signals in wind, precipitation, and solar shortwave radiation are added to the climatological annual cycle during 46 pentad beginning 1 October. Waliser et al. (2003) argued that the mixed layer depth (MLD) shoals during easterly phases and thickens during westerly phases. The shoaling mixed layer is about 20 m thinner than that of the thicker MLD, producing a mean westward current for the event. In the equatorial Indian Ocean, the rectified zonal surface currents in their solution are eastward and very weak (2–6 cm s^{-1}). Causes for the weak currents, however, were not provided by the authors.

In fact, other studies, after Robinson (1966) and Gill (1975), also suggested that nonlinearity of the ocean acts to enhance the eastward transport in the equatorial region. Cane (1980) demonstrated that westerly winds cause equatorial convergence that advects the eastward momentum downward, producing an eastward subsurface flow. In contrast, easterly winds cause equatorial divergence and at the same time build up an eastward pressure gradient force, producing an eastward subsurface current. This eastward subsurface flow is advected upward due to the surface Ekman divergence. Cane (1980) and Pedlosky (1987) also suggested the nonlinear enhancement of eastward transport in an equatorial undercurrent (EUC), considering that the subsurface flow conserves absolute vorticity when it moves toward the equator. In addition, Philander and Pacanowski (1980) showed that upward advection of the EUC in the Pacific Ocean can cause an eastward surface current, and the importance of nonlinear advection in the momentum balance of seasonal cycle was pointed out by McPhaden and Taft (1988), by analyzing time series of surface current data in the eastern equatorial Pacific.

Aside from the low-frequency rectification due to nonlinearity of the oceanic system, Shinoda and Hendon (2002) analyzed 51 years of the National Centers for Environmental Prediction–National Center for Atmospheric Research (NCEP–NCAR) reanalysis and suggested that the MJO can induce low-frequency rectification in wind speed and thus latent heat flux, which are in the forcing fields themselves. These rectified forcing effects were demonstrated to be unimportant by Waliser et al. (2003).

b. Present research

The goal of this paper is to provide a detailed understanding of the low-frequency rectification of atmospheric intraseasonal variability on zonal surface current and transport in the equatorial Indian Ocean, which has not yet been done to date. For this purpose, an ocean general circulation model (OGCM) is used as a primary tool. To help to identify the nonlinear effects, a linear continuously stratified ocean model (LM) is also used: An intermediate ocean model (IOM) is applied to help to quantify various nonlinear processes that cause the low-frequency rectification.

Since the surface currents in the equatorial Indian Ocean are dominated by the eastward surface Wyrtki jets (WJs) during spring and autumn, modification of the WJ strength will have direct impact on the zonal advection of SST, and modification of WJ transport will directly affect the heat storage in the eastern Indian Ocean warm pool and thus may impact the warm pool convection. Additionally, because the autumn WJ is an important component for the Indian Ocean zonal mode (IOZM), the coupled mode of interannual variability in the tropical Indian Ocean (Saji et al. 1999; Webster et al. 1999; Behera et al. 1999; Murtugudde et al. 2000), variations of the WJs may also affect the IOZM events.

The rest of the paper is organized as follows. Section 2 provides a brief description of the ocean models. Section 3 discusses the hierarchy of OGCM, LM, and IOM

experiments designed to understand the impacts of atmospheric intraseasonal variabilities, and to explore the processes involved. Impacts during the IOZM years are separately discussed. Section 4 provides a summary and discussion.

Note that, throughout this paper, ''low frequency'' refers to the seasonal-to-interannual oscillations with period longer than 90 days, ''intraseasonal variability'' refers to the variability with period of 10–90 days, and seasons refer to those of the Northern Hemisphere.

2. Models and experiments

a. HYCOM

Since HYCOM is documented in detail elsewhere (see Bleck 2002), here we only provide a brief description that is essential for our discussion. HYCOM has a hybrid vertical coordinate system, which is isopycnal in the open, stratified ocean but smoothly reverts to a terrain-following coordinate in shallow coastal regions and to *z*-level coordinates in the mixed layer and/or unstratified seas. It intends to integrate the advantages of isopycnic, *z*-level, and terrain-following coordinates and thus can retain its water mass characteristics for centuries, have high vertical resolution in the surface mixed layer, maintain sufficient vertical resolution in unstratified or weakly stratified regions of the ocean, and have high vertical resolution in coastal regions. The feasibility of the hybrid coordinate approach for handling both deep and shallow regions, throughout the annual heating/cooling cycle, has recently been demonstrated for a North Atlantic basin configuration by Halliwell (1998, 2004). The basin model has performed well both in terms of numerical stability and physical realism in a series of multidecadal simulations.

1) INDIAN OCEAN CONFIGURATION

In this paper, HYCOM is configured for the tropical Indian Ocean north of 29°S, with a horizontal resolution of 0.5° × 0.5° and realistic bottom topography. Vertically, 18 layers are chosen with a fine resolution in the upper ocean to better resolve the vertical structures of upper ocean currents, temperature, mixed layer, and thermocline. Reference pressure sigma 0 is adopted because our focus is on the upper Indian Ocean. The nonlocal *K*-profile parameterization (KPP) is adopted for the boundary layer mixing scheme (Large et al. 1994, 1997). The diapycnal mixing coefficient is set to $(1 \times 10^{-7}\ \mathrm{m^2\ s^{-2}})/N$, where N is the buoyancy frequency. Isopycnal diffusivity and viscosity values are formulated as $u_d \Delta x$, where Δx is the local horizontal mesh size and u_d is 0.03 m s^{-1} for momentum and 0.015 m s^{-1} for temperature and salinity. In regions of large shear, isopycnal viscosity is set proportional to the product of mesh size squared and total deformation (Bleck 2002); the proportionality factor here is 0.6. Solar shortwave radiation penetration is included with Jerlov water type IA (Jerlov 1976).

Along the continental boundaries, no-slip boundary conditions are applied. Near the southern boundary, a sponge layer of 4° (25°–29°S) is applied to relax the model temperature and salinity to Levitus and Boyer (1994) and Levitus et al. (1994) climatology. Lateral boundary forcing due to the Indonesian Throughflow is included by relaxing the model temperature and salinity to Levitus data in the throughflow region. Freshwater due to the Bay of Bengal rivers is neglected because only a small portion of the river water reaches the equator and thus its effect on currents and SST is negligible in the equatorial region (Han et al. 2001b; Howden and Murtugudde 2001). The bottom topographic data are from the Earth Topography—5 Minute (ETOPO5) smoothed over a 10° × 10° bin.

2) FORCING AND TIME INTEGRATION

The wind stress, wind speed, air temperature, specific humidity, solar shortwave radiation, and outgoing longwave radiation used to force the OGCM are from the NCEP–NCAR reanalysis for the period of 1988–2001 (Kalnay et al. 1996). This period of time is chosen because it covers two recent IOZM events (1994, 1997), includes the World Ocean Circulation Experiment (WOCE) current measurement period in the equatorial Indian Ocean (1993–94), and is long enough to include interannual variability. Two versions of these forcing fields are utilized: 3-day means, which include intraseasonal variability, and monthly means, which exclude intraseasonal variability. Precipitation is from the Climate Prediction Center (CPC) Merged Analysis of Precipitation (CMAP) pentad and monthly mean rainfall data for the same period of time (Xie and Arkin 1996). We have compared the CMAP pentad data with the 3-day mean Microwave Sounding Unit (MSU) precipitation during their overlapping period of 1979–96. Intraseasonal variability in the two fields agrees very well. Here we choose to use CMAP precipitation because its record covers our entire period of interest. The pentad precipitation is interpolated to the 3-day resolution that corresponds to the 3-day NCEP data.

As can be seen from Fig. 1, NCEP 3-day mean winds (dashed curves) agree well with the research-quality, Center for Ocean–Atmosphere Prediction Studies (COAPS)/Florida State University (FSU) National Aeronautics and Space Administration (NASA) Scatterometer (NSCAT) gridded wind product (solid curves) after both winds are averaged over (5°S–5°N, 50°–90°E) of the equatorial Indian Ocean. The correlation coefficient between the two curves is 0.93 for zonal wind stress (Fig. 1a) and 0.95 for meridional wind stress (Fig. 1b), with a red noise significance above 99.5%. However, the correlation decreases if we first calculate the correlation coefficient on each HYCOM grid point and then average the coefficients over (5°S–5°N, 50°–90°E).

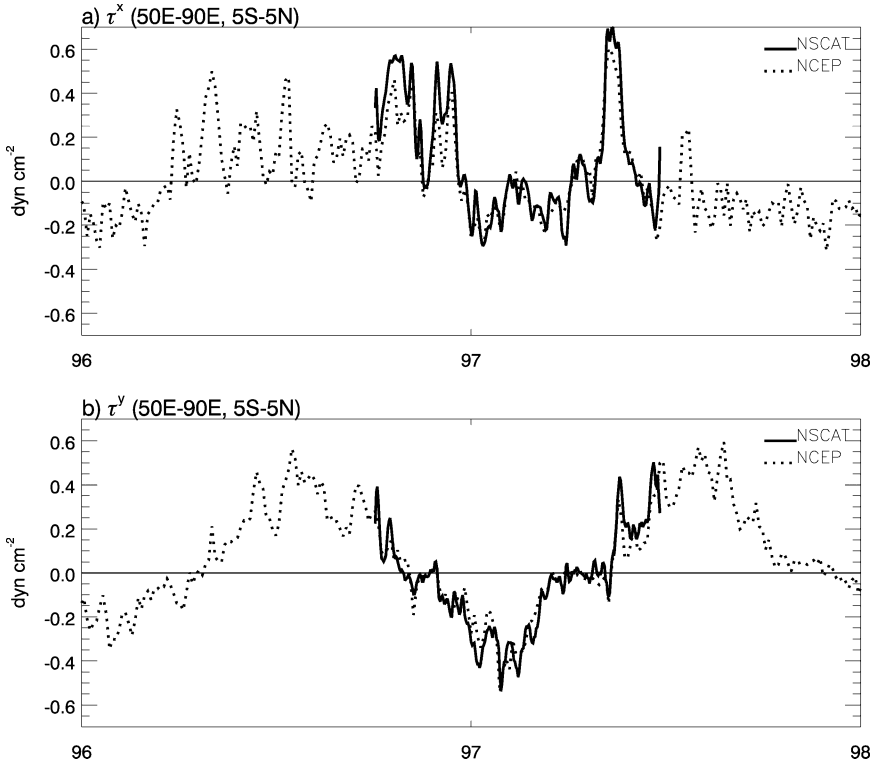

FIG. 1. (a) Time series of 3-day mean zonal wind stress τ^x, averaged over the equatorial Indian Ocean (5°S–5°N, 50°–90°E) from NCEP reanalysis (dashed curves) and from the gridded NSCAT winds (solid curves) during 1996–97. The NSCAT wind stress in the figure is derived from the daily FSU NSCAT pseudostress with a drag coefficient of 0.0013, air density of 1.175 kg m^{-3}, and use of a 3-day running average. (b) As in (a) but for meridional wind stress τ^y. Units: dyn cm^{-2}.

The averaged correlation coefficient is 0.76 (0.71) for zonal (meridional) wind stress, with a red noise significance above 99.5%. These results suggest that, while NCEP and NSCAT winds generally agree, there are certain differences in spatial structure and amplitude during some times of the data period. Nevertheless, given that the NCEP reanalysis did not assimilate the satellite winds and NSCAT accurately determines wind directions as well as wind speeds (Bourassa et al. 1997), the good agreement between the two demonstrates that NCEP winds are generally able to realistically capture the intraseasonal variability and hence serve the purpose of the present study.

Both surface winds and precipitation, the two dominant factors for generating the equatorial surface jets (Han et al. 1999), exhibit large-amplitude intraseasonal fluctuations (Fig. 2, thin solid curves). Amplitudes of intraseasonal perturbations are as strong as, or stronger than, their seasonal variations (dashed curves). Obviously, intraseasonal variations also show significant seasonality and interannual variability, with large-amplitude fluctuations of zonal wind stress generally occurring in spring and autumn. During autumn and winter of 1994 and 1997, when the IOZM events occur, strengths of intraseasonal fluctuations in winds appear to be weaker.

Also shown in Fig. 2a is the 3-day mean wind after a 90-day low-pass filter (thick solid curve), which is a 31-point boxcar running average. The filtered winds are almost identical to the monthly mean winds (dashed curves), suggesting that the monthly mean winds basically filter out the intraseasonal variability and energy at intraseasonal period aliased by the monthly means is negligible. This point is further demonstrated in section 3b(2ii). Consequently, this paper examines the rectified effect due to intraseasonal forcing that does not include the rectified forcing effect discussed by Shinoda and Hendon (2002). This filter will be used to filter out the intraseasonal variability for the OGCM solutions in the next section.

The time step of integration for the barotropic mode is 72 s, and for the baroclinic modes is 2160 s. First, the model is spun up from a state of rest for 20 yr using Comprehensive Ocean–Atmosphere Data Set (COADS) monthly mean climatological fields. Then, starting from the results of year 20, HYCOM is integrated from 1988 to 2001 using the 3-day and monthly forcing fields described above. Considering that the first two years

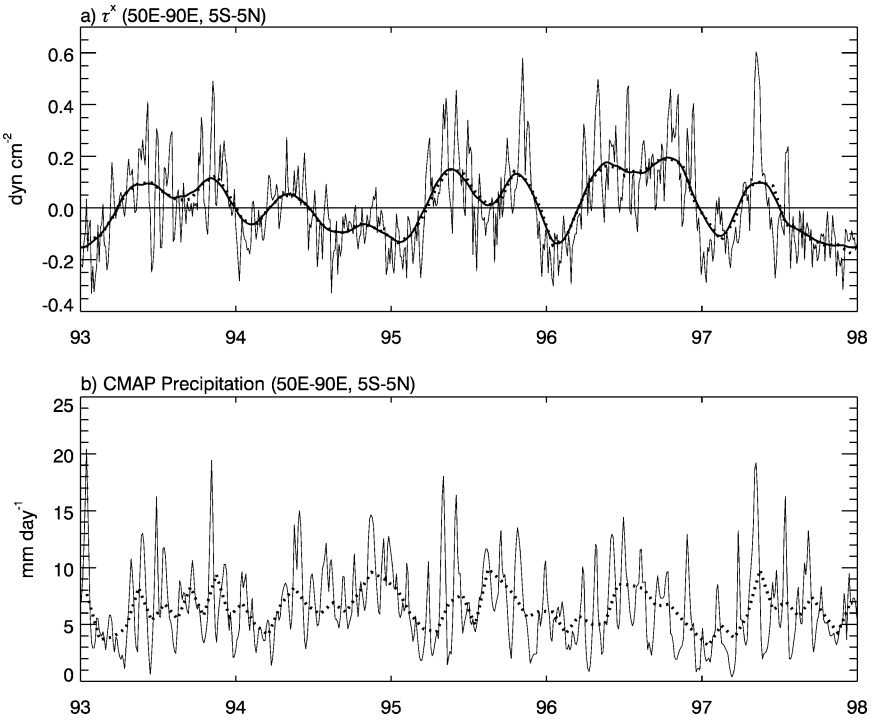

FIG. 2. (a) Time series of the NCEP 3-day mean (thin solid curves) and monthly mean (dashed curves) zonal wind stress averaged over the equatorial Indian Ocean (5°S–5°N, 50°–90°E) during 1993–97. The thick solid curve is the 3-day mean data after 90-day low-pass filtering. Units: dyn cm^{-2}. (b) As in (a) but for the CMAP pentad and monthly precipitation (thick solid and dashed curves). Units: mm day^{-1}.

(1988–89) may include transient effects, results for 1990–2001 are used to calculate the standard deviation of surface current in section 3b(1). In fact, most model results that we show in later sections are for the period of 1993–97.

b. The LM

In this paper, the wind-driven, linear continuously stratified ocean model is used only to help to identify the nonlinear effects. The model is described in detail in McCreary (1980, 1981) and is applied to several Indian Ocean studies, such as Shankar et al. (1996) and McCreary et al. (1996). The equations of motion are linearized about a background state of rest with a realistic stratification, and the ocean bottom is assumed flat. With these restrictions, solutions can be represented as expansions in the vertical normal modes of the system, and the total solution is the sum of all the modes. In this paper, the first 25 baroclinic modes are used and solutions are well converged with this choice. The grid used is $\Delta x = \Delta y = 55$ km, which is close to the 0.5° × 0.5° for HYCOM. The model basin is the realistic Indian Ocean north of 29°S as for HYCOM. It includes representations of the Maldives Islands and Lakshadweep Island with rectangular boxes along 73°–74°E. Along the continental and island boundaries, no-slip boundary conditions are used. The southern boundary is open, and zero-gradient boundary conditions are applied. The linear model is first spun up for 20 years using monthly climatology of COADS wind stress forcing, with a time step of 1 h. Starting from year 20, the model is integrated forward for the period of 1988–2001 using the NCEP 3-day and monthly wind stress forcing, respectively.

c. The IOM

A detailed discussion of the nonlinear, $4\frac{1}{2}$-layer IOM can be found in Han (1999). The model consists of four dynamically active layers that roughly span a few hundred meters of the upper ocean, overlying a deep inert layer where motion is assumed to vanish. Layer 1 represents the surface mixed layer, layer 2 is the seasonal thermocline, layer 3 is the thermocline, and layer 4 is the upper-intermediate water. The mixing scheme for the surface mixed layer is based on the Kraus–Turner mixed layer physics (Kraus and Turner 1967) and is also Richardson number dependent. Layer thicknesses h_1 and h_2 are not permitted to become thinner than minimum values $h_{1\min} = 10$ m and $h_{2\min} = 10$ m. These minima are necessary to keep the model numerically stable. However, solutions are not sensitive to these values provided they are sufficiently small.

The advantage of the IOM is that its simplicity enables us to isolate different processes that are not easy to isolate in the OGCM, and meanwhile it is complicated enough to produce a result that agrees with the observation [section 3c(3)]. For example, entrainment of momentum due to intraseasonal wind forcing in the IOM is caused only by wind speed, which affects the frictional velocity in the Kraus–Turner mixed layer scheme. To eliminate this effect, we can simply remove the intraseasonal wind speed variation in the entrainment term. As we have seen, the IOM is different from HYCOM in various aspects. First, it has only four degrees of freedom vertically, which may exaggerate the effects of entrainment and upwelling. Second, it adopts the Kraus–Turner mixed layer physics, which is different from the KPP mixing scheme used in HYCOM. However, similar rectified low-frequency surface currents appear in both models (section 3), indicating that the rectification of atmospheric intraseasonal variability into the seasonal-to-interannual oceanic variability examined in this study is reliable.

The model basin and grid dimensions are the same as for the LM. The southern boundary is open; zero-gradient boundary conditions with a damper on u_i are applied (see McCreary et al. 1993; Han 1999) except for layers 3 and 4 for which waters that enter the basin have temperatures of 15° and 8°C and salinities of 35.6 and 34.8 psu, respectively. Because the southern boundary is open, two correction ''wedges'' are included in the southwestern corners of the basin to ensure that mass is conserved. One of them, located in layer 3, ensures that mass is conserved in layers 1, 2, and 3; the other, located in layer 4, ensures that mass is conserved in layer 4.

Forcing fields for the IOM are the 5-day mean NCEP–NCAR reanalysis fields during our period of interest, the 90-day low-pass version of the 5-day mean wind stress and speed by applying the Lanczos filter with half power point placed at the 90-day period (Duchon 1979), and idealized intraseasonal winds. The models are integrated forward in time with a time step of $\Delta t = 0.8$ h. The spinup and interannual integrations are the same as those for HYCOM. For the experiments with idealized wind forcing, the model is first integrated forward for 5 years using the 5-day mean NCEP climatologies, and then integrated forward for another 3 years by adding an idealized intraseasonal oscillation to the climatological zonal wind stress. For the basin size of the equatorial Indian Ocean, solutions at the equator responding to the equatorial wind basically reach equilibrium states after a 5-yr spin up since it takes Rossby and Kelvin waves associated with the second baroclinic mode ($c_2 = 167$ cm s^{-1}), the dominant mode in the Indian Ocean, only 0.5 yr to cross the basin back and forth.

d. Experiments

A hierarchy of experiments is performed for each model in order to quantify the impact of atmospheric intraseasonal variability on the seasonal-to-interannual surface current and transport in the equatorial Indian Ocean and to understand the nonlinear processes involved (see Table 1).

To isolate effects of intraseasonal atmospheric forcing, HYCOM is forced by the 3-day mean and monthly fields described in section 2a for the period of 1988–2001, respectively. The former includes the intraseasonal atmospheric forcing and is referred to as the OGCM main run (OGCM_MR); the latter excludes the intraseasonal forcing and is referred to as the OGCM background run (OGCM_BR). To estimate the impact due only to intraseasonal precipitation, intraseasonal variation is removed from the 3-day mean precipitation field by applying the 90-day low-pass filter described in section 2a(2). This solution is referred to as the OGCM no intraseasonal precipitation (OGCM_NOP), and it is found for the period of 1993–97. Similarly, we obtain solution OGCM_NOSW, in which intraseasonal shortwave radiation is removed from the 3-day forcing field. These two aspects are specifically examined because salinity effects due to precipitation can also have a significant influence on the WJs (Han et al. 1999; Masson et al. 2003), and intraseasonal shortwave radiation has been suggested to be important for generating the intraseasonal and rectified SST (Shinoda and Hendon 1998; Waliser et al. 2003).

To help to identify nonlinear effects, the LM is forced by the 3-day and monthly wind stress fields, respectively. These solutions are referred to as LM_MR and LM_BR.

Last, to help to quantify the effects of nonlinear processes, a suite of IOM solutions are found. First, the IOM is forced by the 5-day mean NCEP forcing fields described in section 2c for the period of 1988–2001 and this solution is referred to as IOM_MR. Then the IOM is forced by the 5-day mean fields but with 90-day low-pass wind stress and speed. This solution is called IOM_BR1. To isolate the effect of entrainment due to intraseasonal wind speed (section 2c), solution IOM_BR2 is found. It is the same as IOM_BR1 except that the intraseasonal wind speed remains in the entrainment term. The difference between IOM_BR2 and IOM_BR1 isolates the entrainment of momentum due to intraseasonal wind speed. A set of IOM tests forced by idealized winds are performed to isolate the effects of different nonlinear processes, and they are described in section 3c(3). The first two are listed in Table 1. They are similar to the two runs of Kessler and Kleeman (2000), with one forced by climatological annual cycle and the other add a 60-day oscillation in zonal wind stress.

3. Results

In this section, we first compare solution OGCM_MR with the observations to verify the model performance (section 3a). Then we report a hierarchy of OGCM and

TABLE 1. Experiments performed for understanding the low-frequency zonal surface current and transport rectification of atmospheric intraseasonal forcing in the equatorial Indian Ocean. See text for detailed description.

Expt	Forcing	Duration
OGCM_MR	3-day mean	1988–2001
OGCM_BR	Monthly mean	1988–2001
OGCM_NOP	3-day mean, low-pass 90-day precipitation	1993–97
OGCM_NOSW	3-day mean, low-pass 90-day shortwave radiation	1993–97
LM_MR	3-day wind stress	1988–2001
LM_BR	Monthly wind stress	1988–2001
IOM_MR	5-day mean	1988–2001
IOM_BR1	Same as IOM_MR but with low-pass 90-day stress and speed	1988–2001
IOM_BR2	Same as IOM_BR1 but with intraseasonal wind speed in entrainment	1988–2001
IOM_CLIM	Climatological 5-day mean with low-pass 90-day stress	Year 7
IOM_EXP	Same as IOM_CLIM but adding 60-day zonal wind stress oscillation	Year 7

linear solutions to quantify the low-frequency rectification of atmospheric intraseasonal variabilities in zonal surface current and transport (section 3b). In section 3c we discuss the nonlinear processes that cause the low-frequency rectification. In section 3d we examine the rectified currents during the IOZM events. Last, in section 3e we compare our solutions with the results from the existing studies.

a. Comparison with the observations

The longest current record in the equatorial Indian Ocean during the model integration period is the WOCE data in the central basin (0°, 80.5°E), which lasts for approximately 13.5 months during 1993–94 (Reppin et al. 1999). Zonal currents in the upper 600 m from WOCE and from the OGCM_MR are shown in Fig. 3. The strong autumn WJ during 1993, weak spring WJ of 1994, the strong EUC during March–April 1994, and the reappearing of the EUC in August 1994, are well simulated by HYCOM. On the seasonal time scale, currents are dominated by the semiannual component. Meanwhile, they also exhibit significant intraseasonal fluctuations.

To quantify the comparison, Fig. 4a shows the time series of WOCE zonal current at 50-m depth (solid curve) and HYCOM current in layer 5 (dotted curve) during August 1993–July 1994. This layer is chosen because 50-m depth is located in the fifth layer of the model at the data location during the WOCE period. The OGCM solution agrees reasonably well with the data, with a correlation coefficient of 0.84 above 95% red noise significance. Their intraseasonal components generally agree (Fig. 4b). The correlation coefficient between the two curves is 0.56 with a red noise significance above 95%. Additionally, surface current from solution OGCM_MR agrees well with the observed current in the eastern equatorial Indian Ocean during the

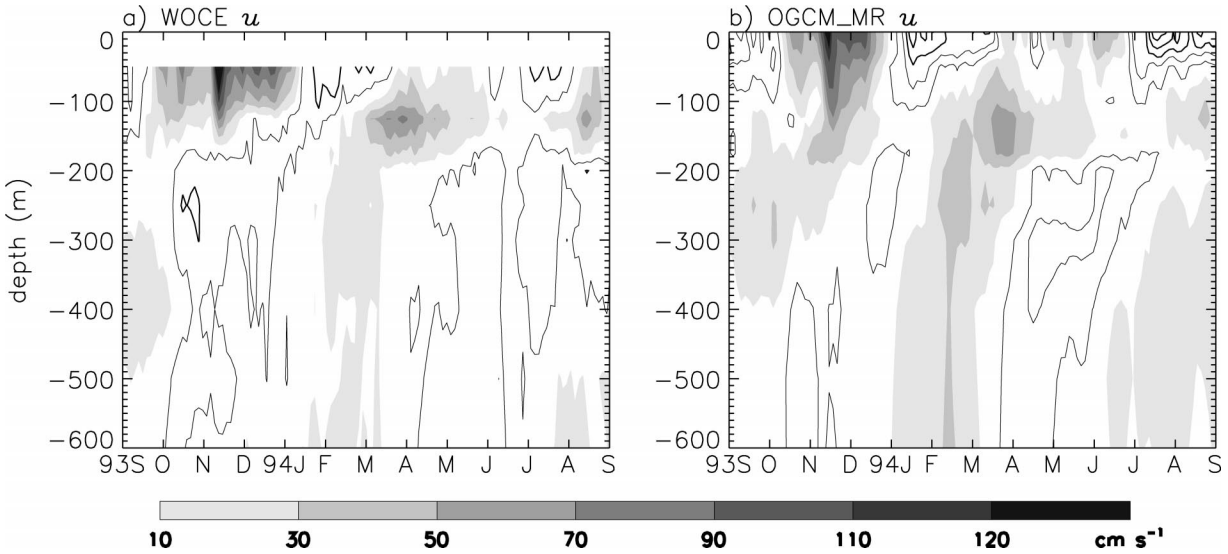

FIG. 3. (a) Observed zonal current u on the Indian Ocean equator (0°, 80.5°E) in the upper 600 m during Sep 1993–Aug 1994 (Reppin et al. 1999); (b) as in (a) but for the OGCM_MR. Positive values are shaded and negative ones are contoured, with an interval of 20 cm s^{-1}. Zero contours are suppressed.

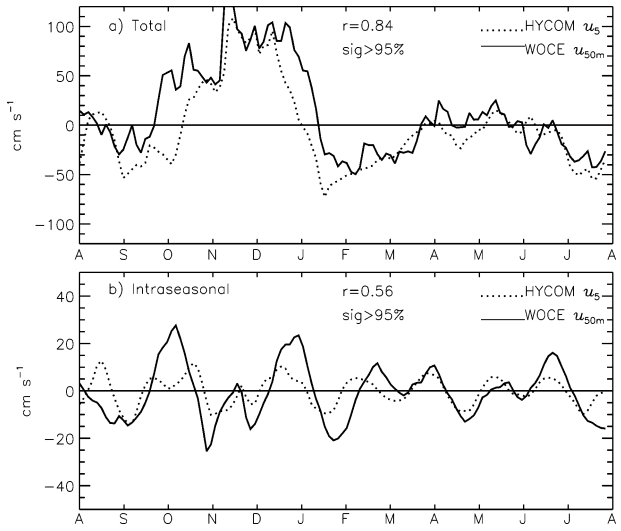

FIG. 4. (a) Observed zonal current at 50-m depth in the central equatorial Indian Ocean (0°, 80.5°E) during Aug 1993–Jul 1994 (solid curve; Reppin et al. 1999), and the corresponding layer-5 current from the OGCM_MR (dashed curve); (b) as in (a) but for the intraseasonal components obtained by removing the annual mean and seasonal components (period longer than 90 days) from the total currents shown in (a). Units: cm s^{-1}.

Joint Air–Sea Monsoon Interaction Experiment (JASMINE; Webster et al. 2002). On the other hand, obvious model/data differences exist (Fig. 4). These differences may result partly from the inaccuracy of the forcing fields [section 2a(2)]. A detailed comparison between the HYCOM solution and the JASMINE data is being carried out by P. Hacker and coauthors.

The good agreement between the model solution and observation suggests that the model is able to reproduce the near-surface zonal flow at intraseasonal-to-seasonal time scales. This correspondence suggests that the model has captured the major physics that determine the zonal currents and their variability and, therefore, it is suitable for the present study.

b. Impact of atmospheric intraseasonal variability

1) SPATIAL STRUCTURE

The observed spatial structure of the WJs was shown in previous studies (Wyrtki 1973; Molinari et al. 1990), and this structure is well reproduced by HYCOM (not shown). Briefly, the WJs are equatorially trapped: They obtain the largest amplitudes at the equator and decrease rapidly toward the north and south.

To understand the overall current structure caused by the intraseasonal forcing, we first calculate the standard deviation of zonal surface currents from the difference solution between OGCM_MR and OGCM_BR (OGCM_MR − OGCM_BR) for the period 1990–2001, the solution that isolates the effect of the intraseasonal forcing. As shown in Fig. 5, current differences with amplitudes greater than 10 cm s^{-1} are present between 10°S and 10°N across the Indian Ocean. The basin-scale maxima occur along the equator where the WJs prevail, suggesting that the intraseasonal atmospheric variability can have a significant impact on the WJs.

2) EQUATORIAL SURFACE CURRENT

Given that modification of the near-surface current can affect the zonal advection of heat, in this section we will focus on examining how the near-surface equatorial current evolves with and without intraseasonal

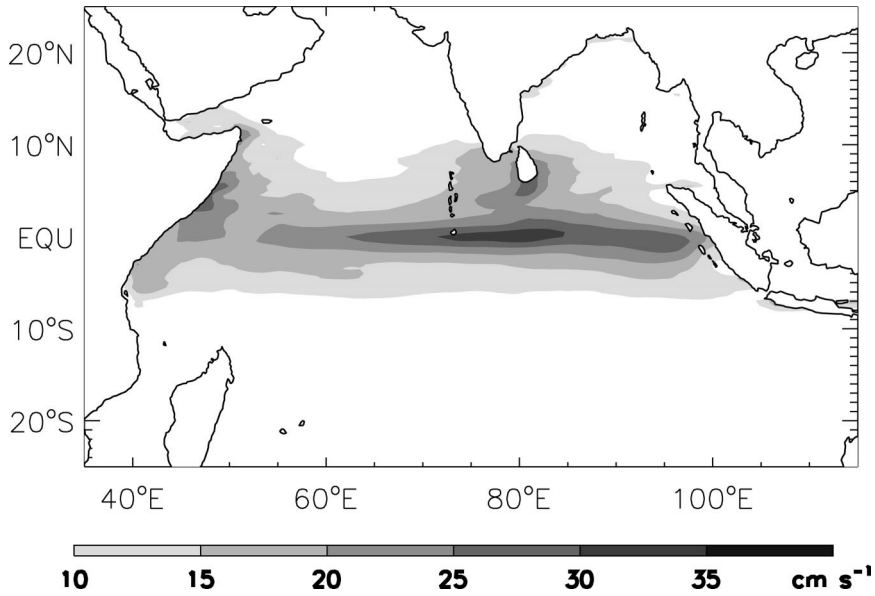

FIG. 5. Standard deviation of mixed layer zonal current u_m from solution OGCM_MR − OGCM_BR for the period 1990–2001. Units: cm s^{-1}.

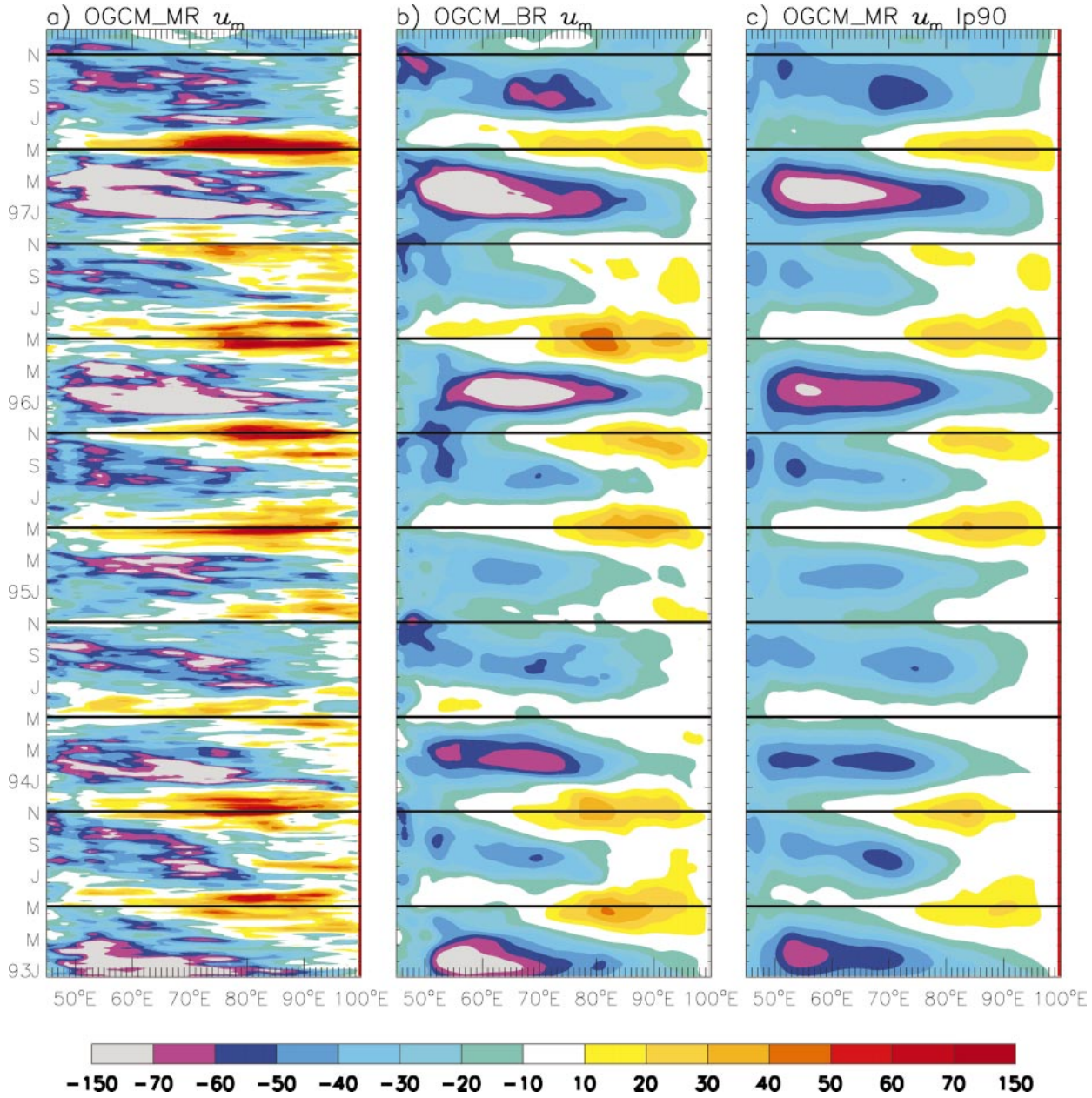

FIG. 6. (a) Longitude–time plot of zonal current in the surface mixed layer, u_m, along the Indian Ocean equator (averaged between 2°S and 2°N) from solution OGCM_MR for the period of 1993–97, the solution that includes intraseasonal forcing. (b) As in (a) but for the current from solution OGCM_BR, which excludes the intraseasonal forcing. (c) As in (a) but after applying a 90-day low-pass filter. Units: cm s^{-1}.

forcing in HYCOM. To this end we examine the current in the well-mixed surface layer, whose depth is defined to be the first depth where the density increase relative to the surface density is equivalent to 0.2°C temperature decrease.

With the intraseasonal atmospheric forcing, the WJs in the surface mixed layer in solution OGCM_MR consist of episodic, swift eastward flow (Fig. 6a) in contrast to the smoothed structure in solution OGCM_BR (Fig. 6b), which is driven by the monthly fields that exclude the intraseasonal impact. Similarly, the westward currents during early spring and summer of each year are composed of episodic, strong westward flow with the intraseasonal forcing. These results suggest that intraseasonal atmospheric variability can generate large amplitude intraseasonal zonal flow in the equatorial Indian Ocean (Han et al. 2001a; Senan et al. 2003), causing significant intraseasonal variability of the equatorial currents. Strengths of the WJs vary from year to year, ranging from over 100 cm s^{-1} to near zero. As a critical

component of the IOZM event, the autumn WJ is especially weak during 1994 and reverses to flow westward during 1997, the two recent IOZM events discussed by a few studies (Saji et al. 1999; Webster et al. 1999; Murtugudde et al. 2000; Vinayachandran et al. 2002).

Of particular interest is that intraseasonal atmospheric forcing not only causes intraseasonal variations in surface flow, but also rectifies into the seasonal-to-interannual currents. After applying the 90-day low-pass filter to the mixed layer current from solution OGCM_MR (Fig. 6c), amplitudes of the filtered WJs are generally weaker than the ones forced by the monthly fields (Fig. 6b), suggesting a low-frequency rectification of surface current by intraseasonal atmospheric forcing. Note that the low-pass filter is applied to the entire time series during the analysis period (1990–2001), but only the 1993–97 currents are shown. The rectified currents during other years have similar features to those in Fig. 6. Additionally, the westward currents during early spring appear to be weakened in Fig. 6c as well.

To further quantify this rectification, Fig. 7a shows the longitude–time plot of the low-frequency currents caused by the intraseasonal atmospheric forcing during 1993–97. To obtain this figure, we first apply the 90-day filter to solution OGCM_MR, which is referred to as ''90-day low-pass OGCM_MR''; then we subtract solution OGCM_BR from solution 90-day low-pass OGCM_MR. Note that, in order to remove the instabilities developed in solution OGCM_BR, a 30-day low-pass filter (11-point boxcar running average) is applied to solution OGCM_BR before the subtraction, and this 30-day low-pass filter is applied to all OGCM_BR solutions shown later. Also plotted in this figure are the thick solid lines across the equatorial basin during the middle of May and November, when the spring and autumn WJs generally reach their peaks. This figure demonstrates that intraseasonal atmospheric forcing acts to weaken the eastward-flowing WJs in most of the equatorial basin, producing westward rectified currents with amplitudes of 5–20 cm s^{-1} during spring and autumn of each year. During early spring, and to a lesser degree during summer, the intraseasonal forcing tends to decrease the westward flow, causing 5–15 cm s^{-1} eastward rectified currents. Consequently, whether the seasonal currents are eastward or westward, high-frequency atmospheric forcing tends to reduce their amplitudes.

While the rectified current amplitude and direction are season dependent, strengths of the rectification vary from year to year. This seasonal-to-interannual variation of the rectified current results primarily from the seasonal-to-interannual change of the background states of the ocean and atmospheric forcing. The seasonal-to-interannual variability of the intraseasonal atmospheric forcing (Fig. 2, thin solid curves) also contributes. This point will be discussed in section 3c(3ii).

(i) Forcing by intraseasonal precipitation and solar shortwave radiation

Since salinity effects due to precipitation were suggested to be influential for the equatorial surface jets (Han et al. 1999), here we isolate and quantify the effects of intraseasonal precipitation. Figure 7b shows the rectified zonal currents in the surface mixed layer due to intraseasonal atmospheric forcing with intraseasonal precipitation removed. It is obtained by applying the 90-day filter to solution OGCM_NOP, the solution that excludes the intraseasonal precipitation but includes other intraseasonal forcing, and then subtract solution OGCM_BR from it. As can be seen from Figs. 7a and 7b, the rectified currents are almost identical with and without the forcing due to intraseasonal precipitation. Similarly, the rectified currents with and without the effect of intraseasonal solar shortwave radiation are almost the same (Figs. 7a,c). These solutions suggest that intraseasonal winds are the primary forcing for generating the low-frequency currents. Rectification effects of intraseasonal precipitation and solar shortwave radiation are negligible. This conclusion is consistent with the results of Waliser et al. (2003), who also showed that intraseasonal variations of precipitation and shortwave radiation had trivial influences on the low-frequency currents, although they were important for the low-frequency SST variability (their Fig. 19).

(ii) Linear solution

The cross-time-scale impact of intraseasonal atmospheric forcing on oceanic currents results from the nonlinearity of the ocean dynamics, because the corresponding low-frequency currents vanish in the linear solution. Figure 7d shows the low-frequency currents from the linear solution caused by intraseasonal wind stress. It is obtained by taking the difference, (90-day low-pass LM_MR) − (LM_BR). Solution LM_MR includes, and LM_BR excludes, the intraseasonal wind stress forcing. The disappearance of the rectified currents in Fig. 7d demonstrates that nonlinear response of the ocean to intraseasonal wind is the major cause for the current rectification. Figure 7d further suggests that the 90-day low-pass filter described in section 2a(2) efficiently removes the intraseasonal variability, and its effect is close to performing the monthly mean since only at very specific occasions there are visible currents due to the aliasing of intraseasonal energy in the monthly mean fields.

3) VOLUME AND HEAT TRANSPORT

Since the volume and hence heat transports of equatorial currents directly affect the heat storage in the Indian Ocean warm pool, in Fig. 8 we quantify the low-frequency rectification of atmospheric intraseasonal forcing in zonal volume and heat transports.

Consistent with earlier studies (Robinson 1966; Gill

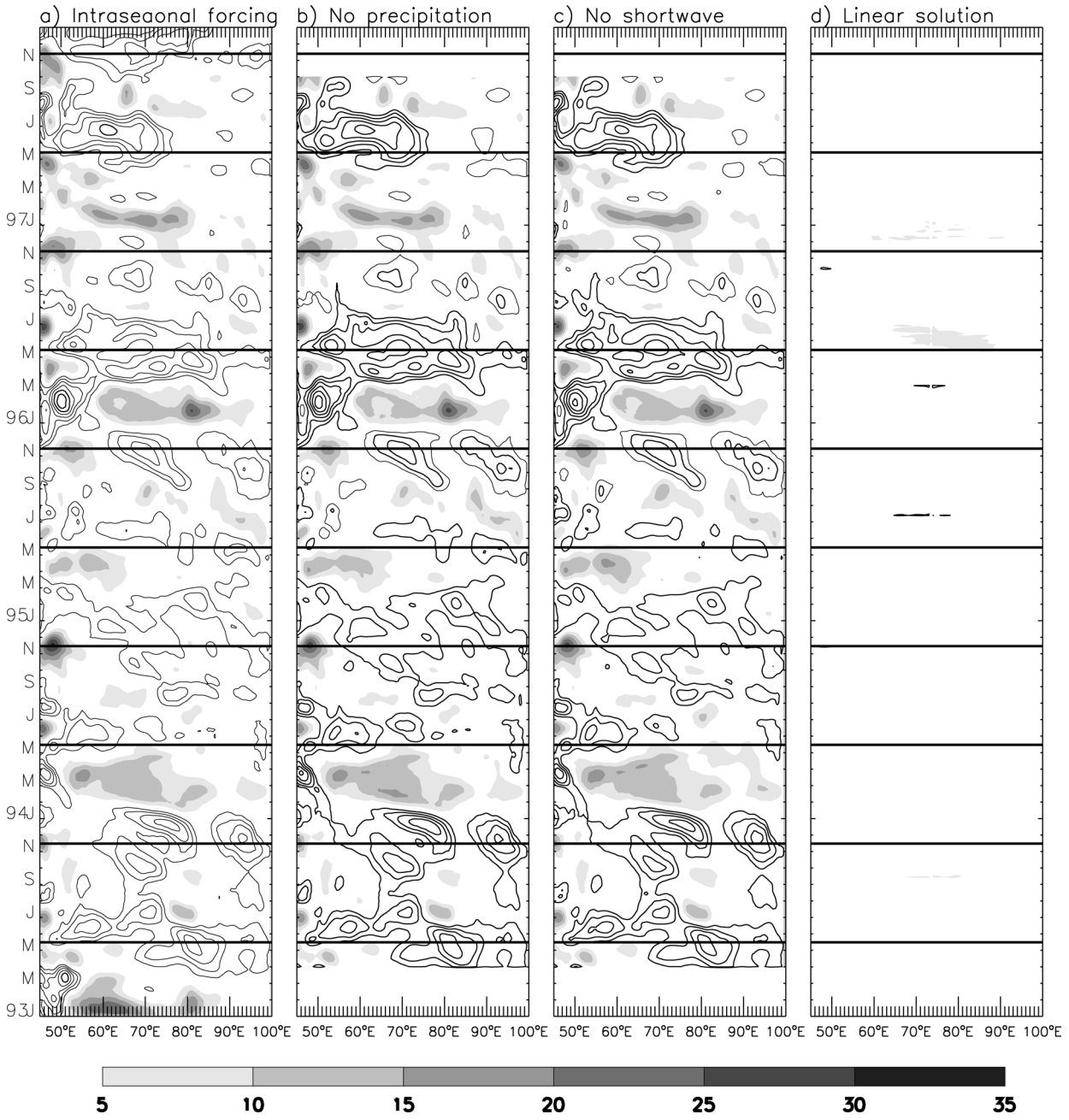

FIG. 7. (a) Longitude–time plot of rectified mixed layer current u_m along the Indian Ocean equator (averaged between 2°S and 2°N), from the difference solution (90-day low-pass OGCM_MR − OGCM_BR) for the period of 1993–97, the solution that isolates the effects of intraseasonal atmospheric forcing; (b) as in (a) except from the difference solution (90-day low-pass OGCM_NOP − OGCM_BR) that isolates the effect of intraseasonal atmospheric forcing other than the intraseasonal precipitation; (c) as in (a) except from the difference solution (90-day low-pass OGCM_NOSW − OGCM_BR) that isolates the effect of intraseasonal atmospheric forcing other than the intraseasonal solar shortwave radiation; (d) low-frequency currents averaged over the upper 20 m from the linear model solution (90-day low-pass LM_MR − LM_BR) that demonstrates that the low-frequency rectification disappears in the linear solution. Positive values are shaded and negative ones are contoured, with an interval of 5 cm s^{-1}. Zero contours are suppressed. Notice that currents during the first 3 months of 1993 and last 3 months of 1997 are not shown in (b) and (c) because of the application of 90-day low-pass filter to solutions OGCM_NOP and OGCM_NOSW. For these two solutions, the OGCM has been run only for the period of 1993–97 (see Table 1).

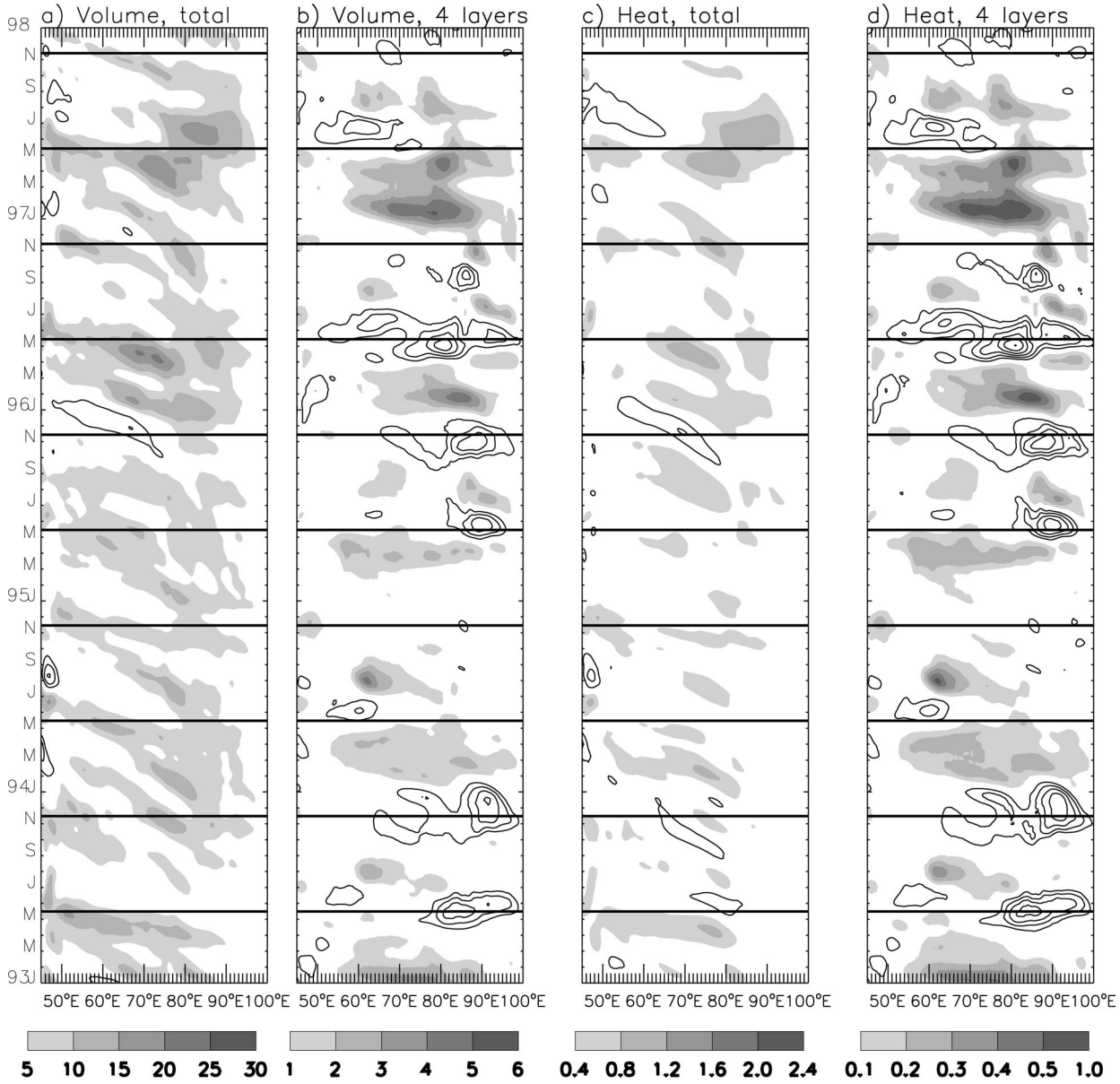

FIG. 8. (a) Longitude–time plot of rectified zonal volume transport along the Indian Ocean equator (averaged between 2°S and 2°N) for the entire water column (sum of all 18 layers), from the difference solution (90-day low-pass OGCM_MR) − (OGCM_BR) for the period of 1993–97; (b) as in (a) but for the upper four layers, which primarily contains the water above the top of the thermocline (22°C isotherm); (c) as in (a) but for zonal heat transport; (d) as in (c) but for the upper four layers. Positive values are shaded and negative ones are contoured, with an interval of 5 Sv for (a), 1 Sv for (b), 0.4 PW (1 PW = 10^{15} W) for (c), and 0.1 PW for (d). Zero contours are suppressed.

1975; Cane 1980; Philander and Pacanowski 1980), the nonlinear response of the ocean to the intraseasonal westerly and easterly winds induces a net eastward vertically integrated volume transport (Fig. 8a), with an amplitude of 0–15 Sv (1 Sv $\equiv 10^6$ m^3 s^{-1}). In the upper ocean above the top of the thermocline (22°C isotherm), however, the rectified zonal transports are westward (eastward) during late spring and autumn (early spring and to a lesser degree during summer, Fig. 8b), which directly follow the rectified surface currents (Fig. 7a). This result suggests that the vertically integrated, persistent rectified eastward transport results largely from the layers in and below the thermocline. Cane (1980) argued that westerly winds drive an eastward equatorial surface current and cause equatorial Ekman convergence and downwelling, which advects the surface eastward momentum downward, causing an eastward subsurface flow. Although westerly winds also cause a westward pressure gradient force, this effect is secondary and acts to weaken the eastward subsurface flow. In contrast, easterly winds cause surface Ekman divergence, meanwhile they produce an eastward pressure

gradient force that drives an eastward subsurface current. This eastward current is advected upward by upwelling driven by the surface divergence. As a result, the net effect of the nonlinear response of the ocean over an intraseasonal cycle tends to produce an eastward vertically integrated transport due to the increased eastward transport below the surface mixed layer.

As expected, the rectified low-frequency heat transports generally have the same signs as the rectified volume transports, both for the vertically integrated case and for the upper ocean above the thermocline (cf. Figs. 8c and 8a, 8d and 8b). Consequently, the rectified, low-frequency vertically integrated heat transport is generally eastward with an amplitude of 0–1.2 PW (Fig. 8c). In the upper ocean above the thermocline, which in the central and eastern equatorial basin mainly contains the warm pool water, the rectified heat transport is season dependent and has a significant interannual variability (Fig. 8d), as the volume transport (Fig. 8b). The rectified seasonal-to-interannual heat transports can directly cause seasonal-to-interannual variations in the warm pool heat storage, which may potentially impact the warm pool convection.

While the rectified eastward transport can be explained by existing theory, the processes that determine the rectified surface currents have not yet been carefully examined.

c. Nonlinear processes for rectified surface current

Processes that can cause rectification of zonal momentum in the surface mixed layer are asymmetric response of MLD to easterly and westerly winds ($\tau^x/h_m\rho_0$), vertical advection (wu_z) and entrainment ($w_e u_z$) of the subsurface water into the surface mixed layer, and horizontal advection (uu_x and vu_y). In the above, τ^x is the zonal wind stress, h_m is the mixed layer thickness, $\rho_0 = 1$ g cm^{-3} is an average density of seawater; u, v, and w are the zonal, meridional, and vertical velocities; and w_e is the entrainment rate. We will first discuss these processes in the OGCM solution and quantify their effects when possible. Then we will analyze a suite of IOM solutions that is designed to estimate the effect of each process.

1) OGCM SOLUTION: $\tau^x/h_m\rho_0$

The episodic westerly winds cause equatorial convergence and downwelling, thus deepening the mixed layer (not shown). On the other hand, the episodic easterly winds cause equatorial divergence and, thus, tend to shoal the mixed layer. Even when the easterly and westerly winds have the same amplitude during one intraseasonal event, there may be a net westward surface current over an event mean because the easterly wind may act on a thinner mixed layer, whereas the westerly wind may act on a much thicker one. This nonlinear effect does not require a low-frequency rectification in the mixed layer depth. That is, the amplitude of mixed layer shoaling during easterly wind does not need to be larger than the mixed layer deepening during westerly wind. As we shall see below, this effect cannot be separated from the entrainment influence due to the intraseasonal wind speed change, which may act to enhance or reduce the asymmetric MLD response depending on the seasonal background state.

Figure 9a shows the rectified mixed layer thickness, h_m, during 1993–97. Like the rectified currents, it is obtained by first applying the 90-day low-pass filter to solution OGCM_MR and then subtracting solution OGCM_BR. The low-frequency rectification of MLD is only 5 m or less, in general, and is positive during some years (such as spring of 1996 and 1997 near 60°E) when the rectified current increments due to $\tau^x/h_m\rho_0$ at a 3-day interval ($\Delta t = 3$ days) are strong and westward (Fig. 9b). Comparison between Figs. 7a and 9b suggests that large impact of the asymmetric MLD response occurs during spring and autumn, and it is an important factor for generating the westward rectified surface current that weakens the spring and autumn WJs. During spring and autumn the seasonal winds are westerlies (Fig. 2a, dashed curve). The westerly phase of an intraseasonal event increases the seasonal westerly wind speed (Fig. 2a, thin solid and dashed curves), increasing entrainment and thus deepening the mixed layer; easterly phase decreases the westerly wind speed or even produces a weak easterly wind, reducing entrainment and hence thinning the mixed layer. This entrainment effect on h_m tends to enhance the h_m change due to the asymmetric response of the MLD, therefore producing a significant westward current rectification over an intraseasonal event mean. This result suggests that the seasonal background state of winds is important for determining the rectified surface currents.

The effect of entrainment on h_m, however, counteracts the asymmetric MLD response during early spring (Fig. 9b) when the seasonal winds are easterlies. This is because, when westerly (easterly) wind of an intraseasonal event tends to deepen (shoal) the mixed layer by causing equatorial Ekman convergence (divergence), the reduced (enhanced) seasonally easterlies act to thin (thicken) the mixed layer. These two effects counteract and entrainment sometimes dominates over the asymmetric MLD response, producing a weak eastward rectified flow (Fig. 9b) that contributes somewhat to the eastward current rectification at this time of the year (Fig. 7).

2) OGCM SOLUTION: ADVECTION AND ENTRAINMENT

Obviously, the asymmetric response of the ocean to westerly and easterly winds cannot explain the strong eastward rectified currents during January–March, which have comparable amplitudes to the low-frequency westward flow, suggesting the importance of other nonlinear processes. Next, we will discuss vertical advec-

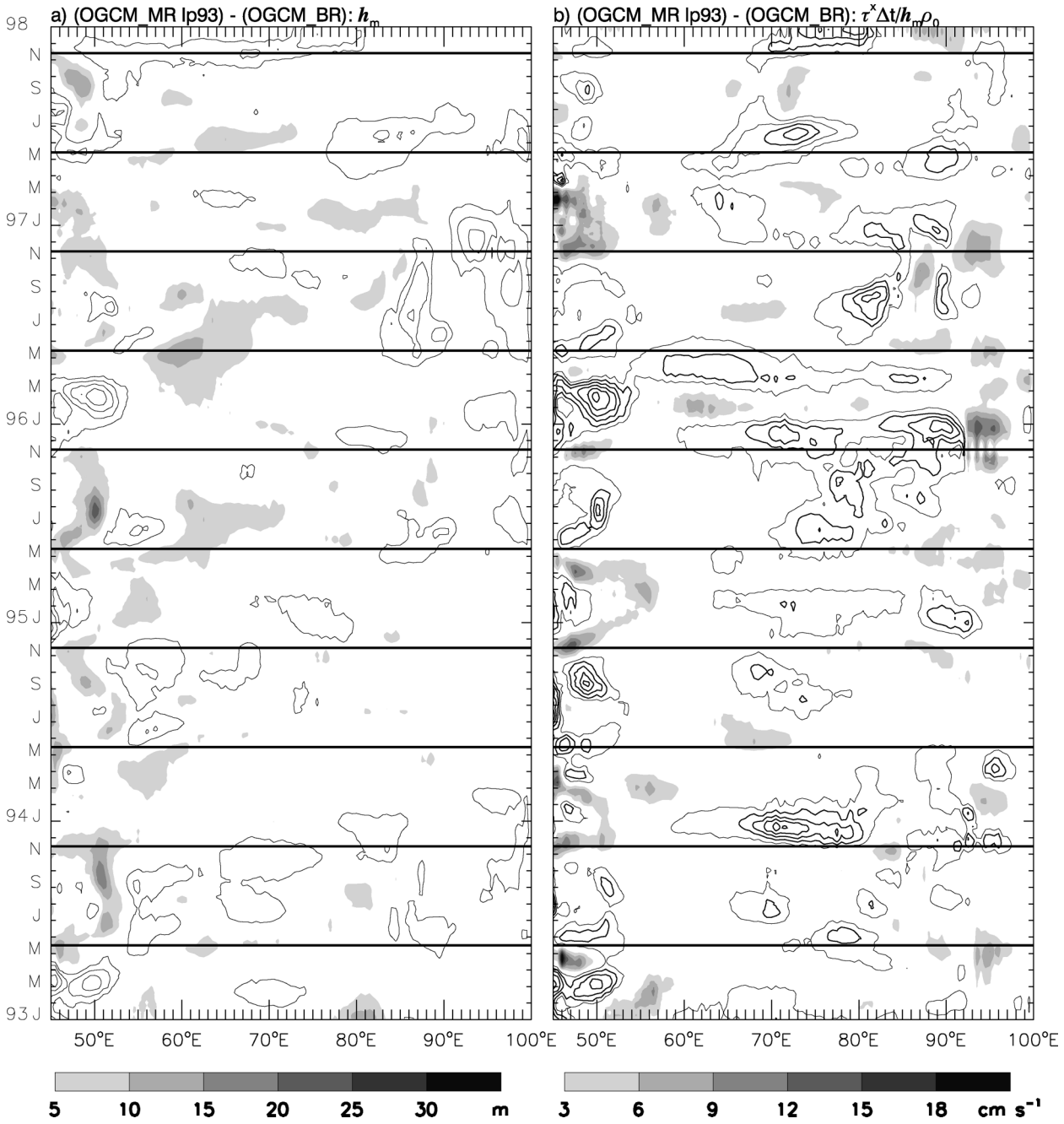

FIG. 9. (a) Rectified mixed layer thickness, h_m, from the difference solution (90-day low-pass OGCM_MR) − (OGCM_BR) for the period of 1993–97, the solution that isolates the effect of intraseasonal atmospheric forcing; (b) as in (a) but for the current increment due to $\tau^x/h_m\rho_0$ for a 3-day interval, $\tau^x\Delta t/h_m\rho_0$, where $\Delta t = 3$ days. Positive values are shaded and negative ones are contoured, with an interval of 5 m for h_m and 3 cm s^{-1} for $\tau^x\Delta t/h_m\rho_0$. Zero contours are suppressed.

tion and entrainment of zonal momentum, using the WOCE observational location and period as an example. Figure 10 shows the current increment due to upward momentum advection, $wu_z\Delta t$ as $w > 0$ and $\Delta t = 3$ days, from solution OGCM_MR (Fig. 10a) and OGCM_BR (Fig. 10b) in the upper 150 m at (0°, 80.5°E) during the WOCE period. Also plotted in each figure is the mixed layer depth from each solution (thick solid curve). From January to March, episodic easterly winds produce significant episodic upward motions across the mixed layer base (shaded regions of Fig. 10a). The positive vertical velocities carry the eastward EUC with them (Fig. 3), causing an eastward surface current anomaly (Fig. 7a). In contrast, the upward motion is very weak without the

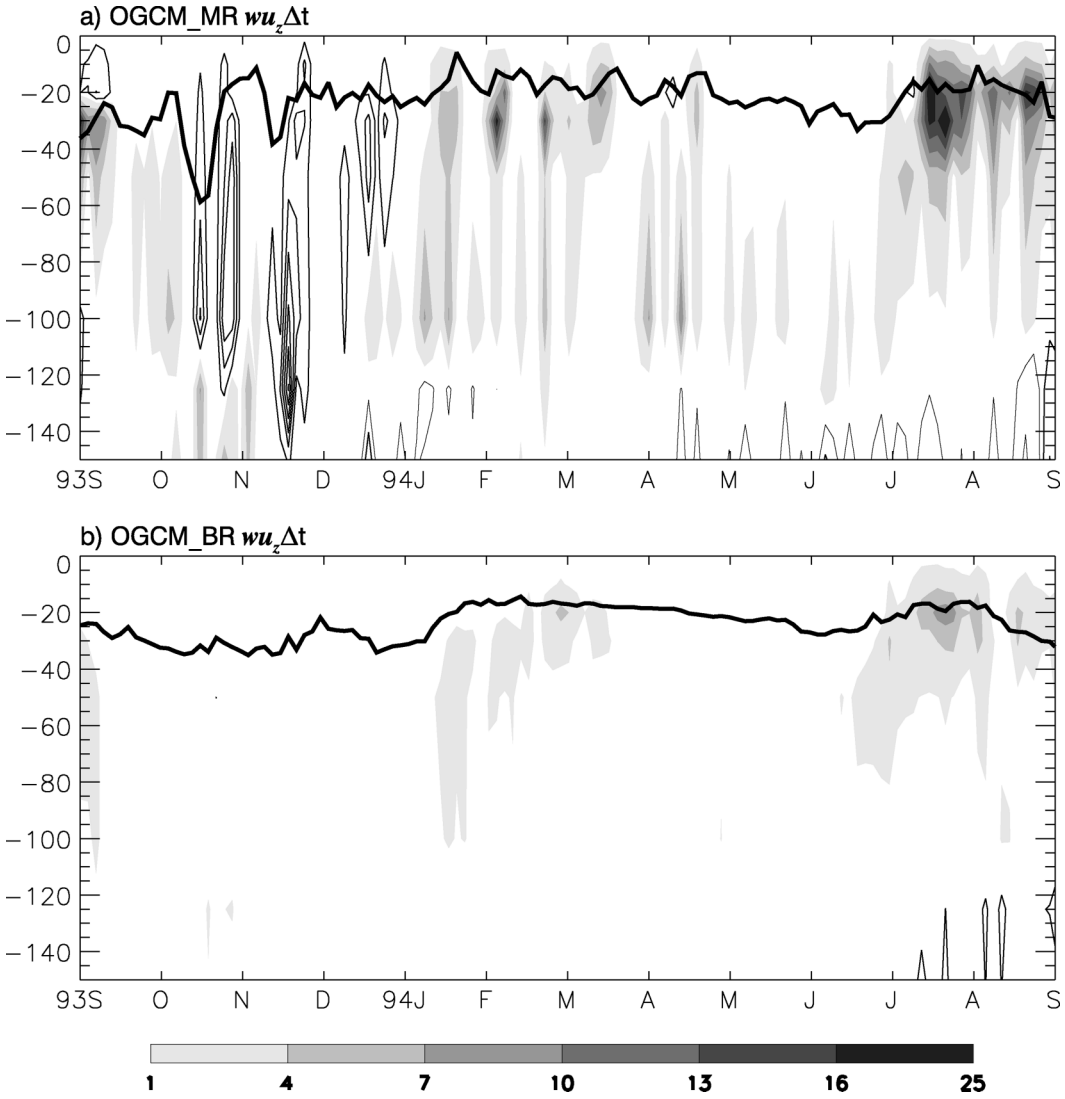

FIG. 10. (a) Current increment due to upward advection of zonal momentum for a 3-day interval, $wu_z\Delta t$ as $w > 0$ and $\Delta t = 3$ days, from OGCM_MR in the upper 150 m at the WOCE current-meter location (0°, 80.5°E) during Sep 1993–Aug 1994. Also plotted in this figure is the mixed layer depth h_m from OGCM_MR (thick solid curve); (b) as in (a) but for solution OGCM_BR. Positive values are shaded, and negative ones are contoured, with an interval of 3 cm s^{-1}. Zero contours are suppressed.

intraseasonal forcing (Fig. 10b), and therefore the upward advection of the EUC is weak in solution OGCM_BR. This result indicates that the seasonal background state of currents is crucial in determining the current rectification.

Additionally, while the strong episodic westerly (easterly) winds during spring and autumn (January–March) thicken (thin) the h_m, the enhanced wind speeds increase the entrainment of the subsurface water. This effect reinforces the westward rectified currents during spring and autumn by entraining the slower subsurface water into the surface mixed layer and enhances the eastward rectification during January–March. This effect, however, is difficult to quantify in the OGCM solutions, and isolating the influences of horizontal advection is not straightforward.

3) IOM SOLUTION

To estimate the contribution from each nonlinear process discussed above, a suite of IOM solutions is found. A similar plot as in Fig. 4 but for the IOM solution shows that the model mixed layer current compares favorably with the 50-m-depth WOCE data, a depth generally within the IOM mixed layer, with a model–data correlation coefficient of 0.82 for the total currents and 0.52 for the intraseasonal components (not shown), in comparison with 0.84 and 0.56 for the OGCM solution.

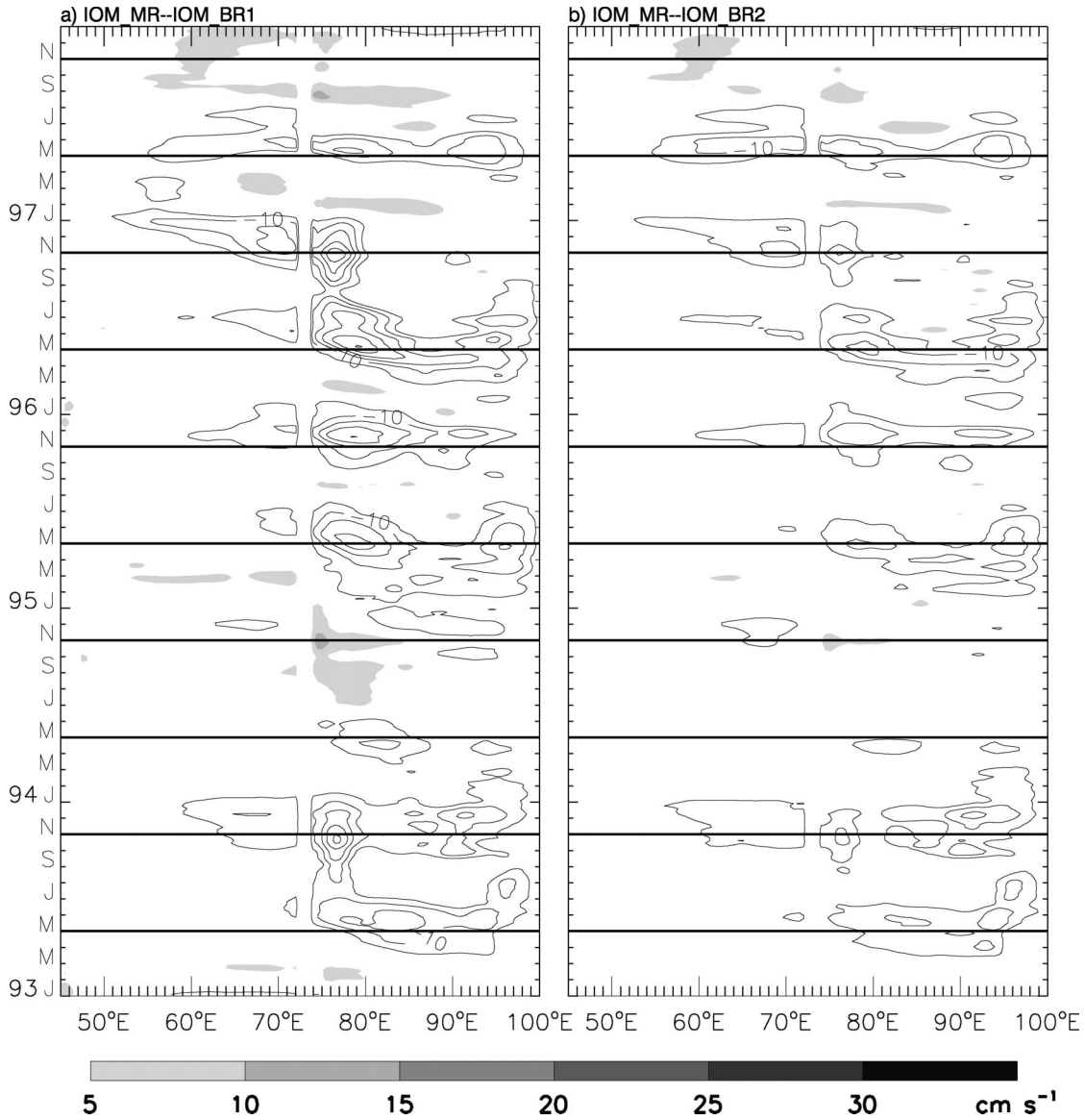

FIG. 11. (a) Longitude–time plot of the rectified currents from the IOM due to intraseasonal wind forcing along the Indian Ocean equator (averaged between 2°S and 2°N) for the period of 1993–97. It is obtained by first finding the difference solution IOM_MR − IOM_BR1 and then performing a 90-day running mean. (b) As in (a) but for solution IOM_MR − IOM_BR2, which isolates the intraseasonal wind stress forcing and excludes the effect of momentum entrainment. Difference between (a) and (b) isolates the entrainment of momentum due to intraseasonal wind speed forcing. Positive values are shaded and negative values are contoured, with an interval of 5 cm s^{-1}. Zero contours are suppressed.

Note that the current discontinuity near 73°E is caused by the representation of the Maldives Islands in the IOM. Effects of the Maldives Islands on the equatorial waves were discussed in detail by Han et al. (1999).

As in the OGCM, the IOM produces westward rectified currents during late spring and autumn (Fig. 11a) and eastward current rectification during January–March. Given the different mixed layer schemes between the two models (section 2), their consistency confirms the rectification effects shown in the OGCM, although there are quantitative differences in amplitudes between the two solutions (Figs. 11a and 7a). Note that only intraseasonal wind stress and wind speed effects are included in Fig. 11a since the OGCM solutions suggested that intraseasonal precipitation and solar shortwave radiation have negligible influence (Fig. 7).

(i) Entrainment due to changes in wind speed

As is suggested in section 3c(2), entrainment acts to enhance the rectification effects, and this is indeed the case. Figure 11b is the same as Fig. 11a except that the

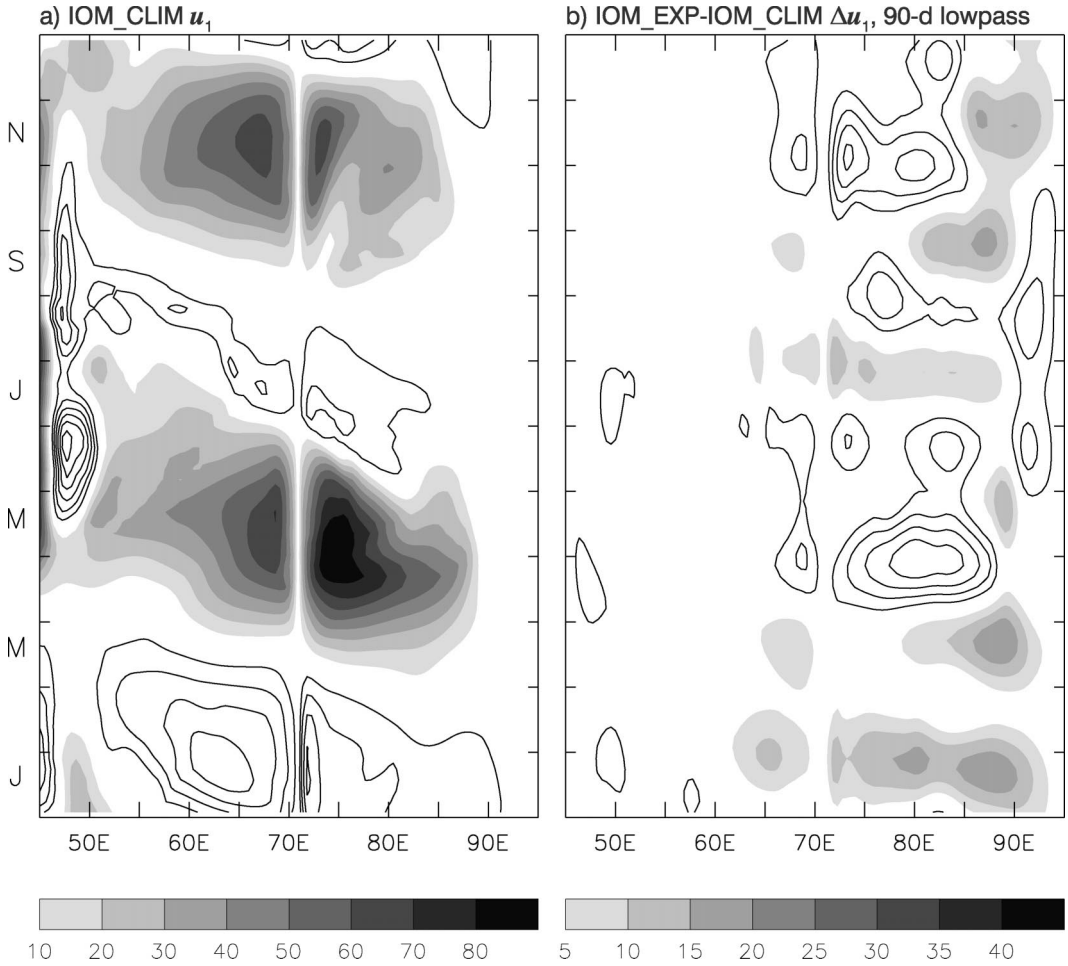

FIG. 12. (a) Longitude–time plot of zonal surface current u_1 from solution IOM_CLIM, the solution with no intraseasonal wind stress forcing; (b) as in (a) but for solution IOM_EXP − IOM_CLIM after performing a 90-day running mean, representing the low-frequency current generated by a 60-day zonal wind stress oscillation. Positive values are shaded and negative values are contoured, with an interval of 10 cm s^{-1} for (a) and 5 cm s^{-1} for (b). Zero contours are suppressed.

effects of entrainment due to intraseasonal wind speed variations are excluded (see section 2d). Amplitudes of both the westward and eastward rectified currents are significantly reduced without the entrainment due to intraseasonal wind speed forcing, demonstrating that the enhanced episodic westerly and easterly winds increase the entrainment of the subsurface water into the surface mixed layer and therefore strengthening the rectified surface currents.

(ii) Advection

A series of tests using idealized wind forcing are performed to estimate the effects of vertical and horizontal advection. First, we force the IOM by 5-day mean NCEP climatological seasonal cycle, except that we apply a low-pass 90-day filter to the wind stress field before forming the climatology. This solution tends to produce the climatological WJs that are independent of the intraseasonal windstress forcing, and it is referred to as the IOM climatological run (IOM_CLIM). Then we add an idealized 60-day oscillation to the low-passed zonal wind stress. The 60-day wind stress has a maximum amplitude of 1 dyn cm^{-2} at 80°E on the equator decreasing as a cosine function to zero at 60°E to the west, 100°E to the east, 5°N to the north, and 5°S to the south. This solution is referred to as IOM_EXP. The difference solution, IOM_EXP − IOM_CLIM, estimates the impact of the pure 60-day wind stress forcing. Idealized intraseasonal wind stress with periods of 45, 50, and 70 days have also been tested, and all produce similar results as the 60-day oscillation does.

As shown in Fig. 12, the additional forcing by the 60-day zonal wind stress produces a low-frequency component that weakens the WJs, reducing the WJ amplitudes by as much as 20 cm s^{-1}. This value is comparable to the currents caused by the realistic intraseasonal wind stress (Fig. 11b). During January–March, and to a lesser degree during summer, seasonal surface

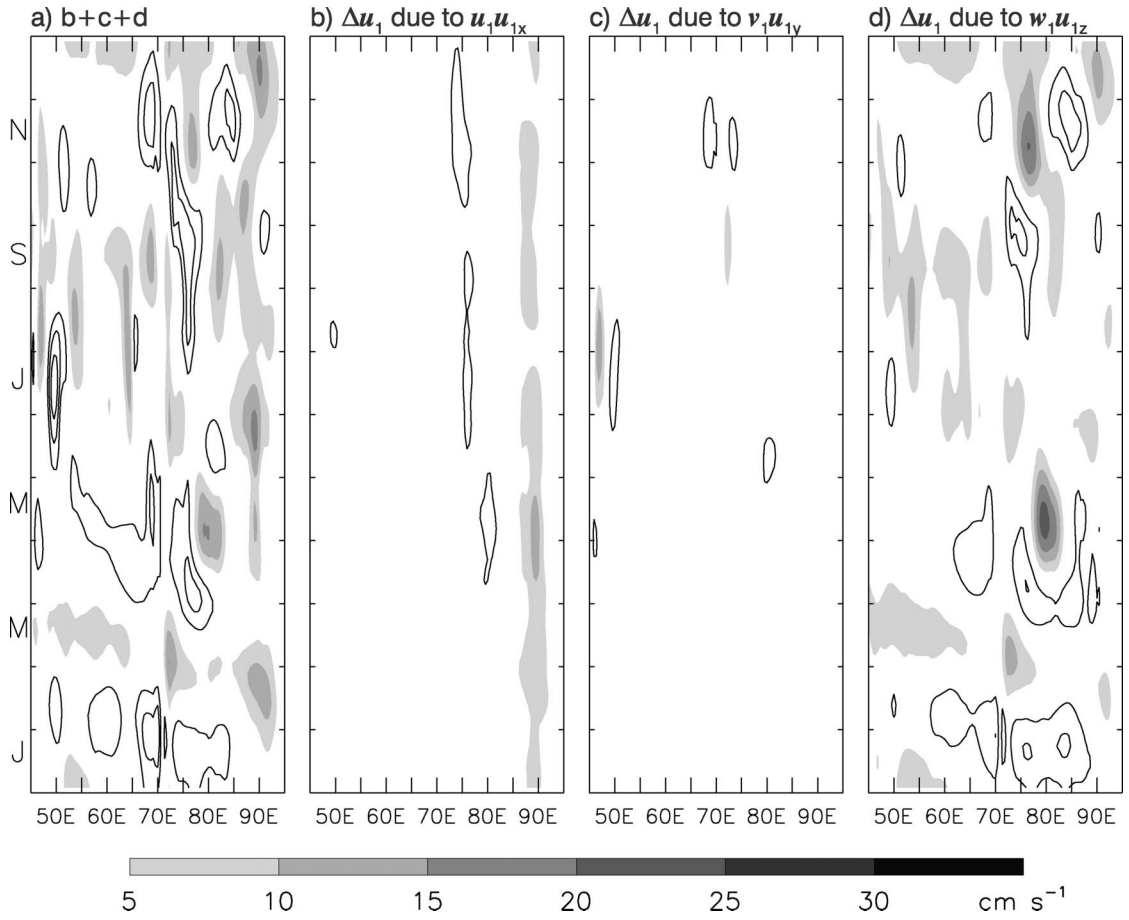

FIG. 13. As in Fig. 12b but for the current caused only by (a) the sum of advection terms $u_1u_{1x} + v_1u_{1y} + w_1(u_1 - u_2)H(w_1)/h_1$, (b) zonal advection u_1u_{1x} term, (c) meridional advection v_1u_{1y} term, and (d) vertical advection $w_1(u_1 - u_2)H(w_1)/h_1$ term. Units: cm s^{-1}.

currents are westward (Fig. 12a) and the rectified currents are eastward (Fig. 12b), consistent with the OGCM and IOM results forced by the realistic forcing fields. Note that in Fig. 12b, the rectified current is caused by a pure 60-day zonal wind stress oscillation whose amplitude does not change with season. In this case, the seasonal dependence of the rectified surface current results from the seasonal cycle of winds on which the 60-day oscillation overlies and from the seasonal cycle of the current background state. This result suggests that the seasonal-to-interannual variabilities of the current and wind background states are crucial in producing the seasonal-to-interannual variation of the rectified surface current. In an IOM test with the amplitude of 60-day wind stress reduced to 0.5 dyn cm^{-2} the rectified currents are reduced (not shown), suggesting that seasonal-to-interannual variability of intraseasonal winds also contributes to the rectified surface current amplitude.

A hierarchy of solutions similar to IOM_CLIM and IOM_EXP is found, but with advection terms, u_1u_{1x}, v_1u_{1y}, and $w_1(u_1 - u_2)H(w_1)/h_1$ successively removed. In the above, $H(w_1)$ is a step function ($H = 1$ when $w_1 > 0$, and $H = 0$ otherwise). Subscripts ''1'' and ''2'' indicate layer indexes of the IOM. The rectified current from solution (IOM_EXP − IOM_CLIM) minus that from the corresponding solution but with u_1u_{1x} term removed isolates the effect of u_1u_{1x}. Effects of other nonlinear terms are obtained in a similar manner. Figure 13 shows the rectified currents due to each of the advection terms (Figs. 13b–d) and their sum (Fig. 13a). Both vertical and horizontal advections contribute to the weakened WJs, with vertical advection playing an important role. The eastward rectification during early spring results primarily from vertical advection, consistent with our discussion in section 3c(2).

(iii) $\tau^x/h_1\rho_0$

Similar to the OGCM solutions, intraseasonal wind stress also produces a westward current rectification during spring and autumn due to the asymmetric response of the ocean to easterly and westerly winds, which acts to weaken the WJs (Fig. 14). During January, this effect accounts for the eastward current rectification in Fig. 12b.

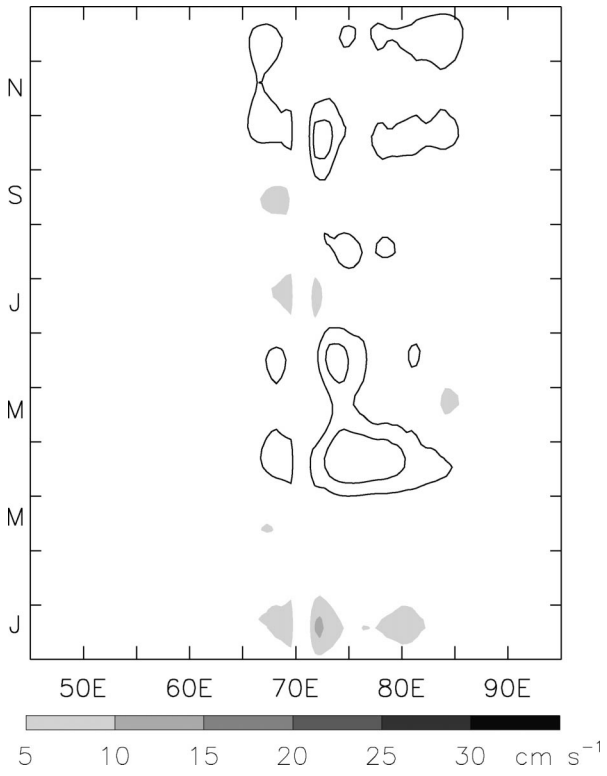

FIG. 14. Longitude–time plot of estimated zonal surface current change caused by the 60-day zonal wind stress oscillation due to the nonlinear forcing term $\tau^x/h_1\rho_0$ calculated from the 5-day mean results of τ^x and h_1 from solutions IOM_EXP and IOM_CLIM. It is obtained by subtracting the $\tau^x\Delta t/h_1\rho_0$ of solution IOM_CLIM from solution IOM_EXP and then performing a 90-day running mean. Here Δt = 5 days. Note that τ^x in solution IOM_CLIM is the low-pass 90-day wind stress whereas τ^x in solution IOM_EXP is the low-pass 90-day wind stress plus an idealized 60-day oscillation. Units: cm s^{-1}.

d. Impact during the IOZM events

In contrast to the equatorial Pacific and Atlantic Oceans where the EUC persists throughout the year, in the equatorial Indian Ocean the EUC is generally observed only during spring (February–April) when easterly winds prevail in most of the equatorial basin. During summer and autumn of 1994 and 1997 when the IOZM events occur, easterly wind anomalies during July–December are so strong that they considerably weaken, or even eliminate, the normally westerly winds during these seasons. The easterly wind drives a westward surface current and at the same time forces an eastward EUC below the surface mixed layer during August–December (Figs. 15a–d), accounting for the observed EUC reappearance during August 1994 (Fig. 3; Reppin et al. 1999). Figure 15 suggests that during IOZM events, the EUC forms in August and lasts through the peak of the events (September–December). The EUC shoals in the eastern basin accompanied by a shallower surface mixed layer (Figs. 15b,d), reflecting a strong upwelling during the IOZM events in the eastern equatorial Indian Ocean. The EUCs during summer and autumn do not occur in normal years, such as 1996 (Figs. 15e,f).

During the peak of the IOZM events (September–December of 1994 and 1997), intraseasonal winds produce a westward rectification in surface currents and heat transports, although their amplitudes are not large (Figs. 7a and 8d). The westward currents result from the asymmetric response of the ocean to intraseasonal winds (Fig. 9b), and this effect dominates the increased entrainment and upwelling that tend to bring the EUC upward, countering the $\tau^x/h_m\rho_0$ effect. Given that intraseasonal winds appear to be weaker in amplitudes during the IOZM (Fig. 2a; T. Shinoda and W. Han 2004, unpublished manuscript) their impact on the IOZM may not be large in comparison with their impacts during normal years.

The intraseasonal forcing, however, produces a basinwide cooling in the equatorial Indian Ocean (not shown). This cooling may result partly from the increased latent heat fluxes. However, our results also suggest that rectified westward flow may enhance the westward advection of the colder, sea surface temperature anomaly (SSTA) associated with the IOZM. Meanwhile, enhanced entrainment due to the intraseasonal wind forcing may also contribute to the cooler SST. A detailed understanding of the intraseasonal impact on the IOZM is beyond the scope of this paper but is an essential part of our ongoing research.

e. Comparison with existing studies

Kessler and Kleeman (2000) obtained an eastward current rectification in the western equatorial Pacific Ocean (their Fig. 3). This result is consistent with our OGCM solutions in the equatorial Indian Ocean during January–March when the rectified currents are eastward (Fig. 7). During this time of the year, surface winds are easterlies and force a westward surface current and an eastward EUC, similar to the equatorial Pacific Ocean. This similarity suggests that enhanced entrainment and upward advection of the EUC may explain the eastward rectification in the Kessler and Kleeman (2000) solution.

The time mean of the anomalous currents caused by the MJO produces a weak but also eastward rectification in the equatorial Indian Ocean in Waliser et al. (2003). Note that the mean was over the MJO forcing period (October–April), and so the weak eastward current rectification (Fig. 19 of Waliser et al. 2003) may represents the average of the rectified westward current during autumn and eastward current during early spring in our OGCM solution (Fig. 7a). It is not clear, however, why the rectified surface currents are westward in the equatorial Pacific in Waliser et al. (2003). Our results suggest that westward currents caused by the asymmetric response of the ocean to easterly and westerly winds may dominate over vertical advection and entrainment of the EUC in the Waliser et al. (2003) solution. Note that this paper examines all intraseasonal forcings, whereas the previous studies tended to isolate the effects of the MJO.

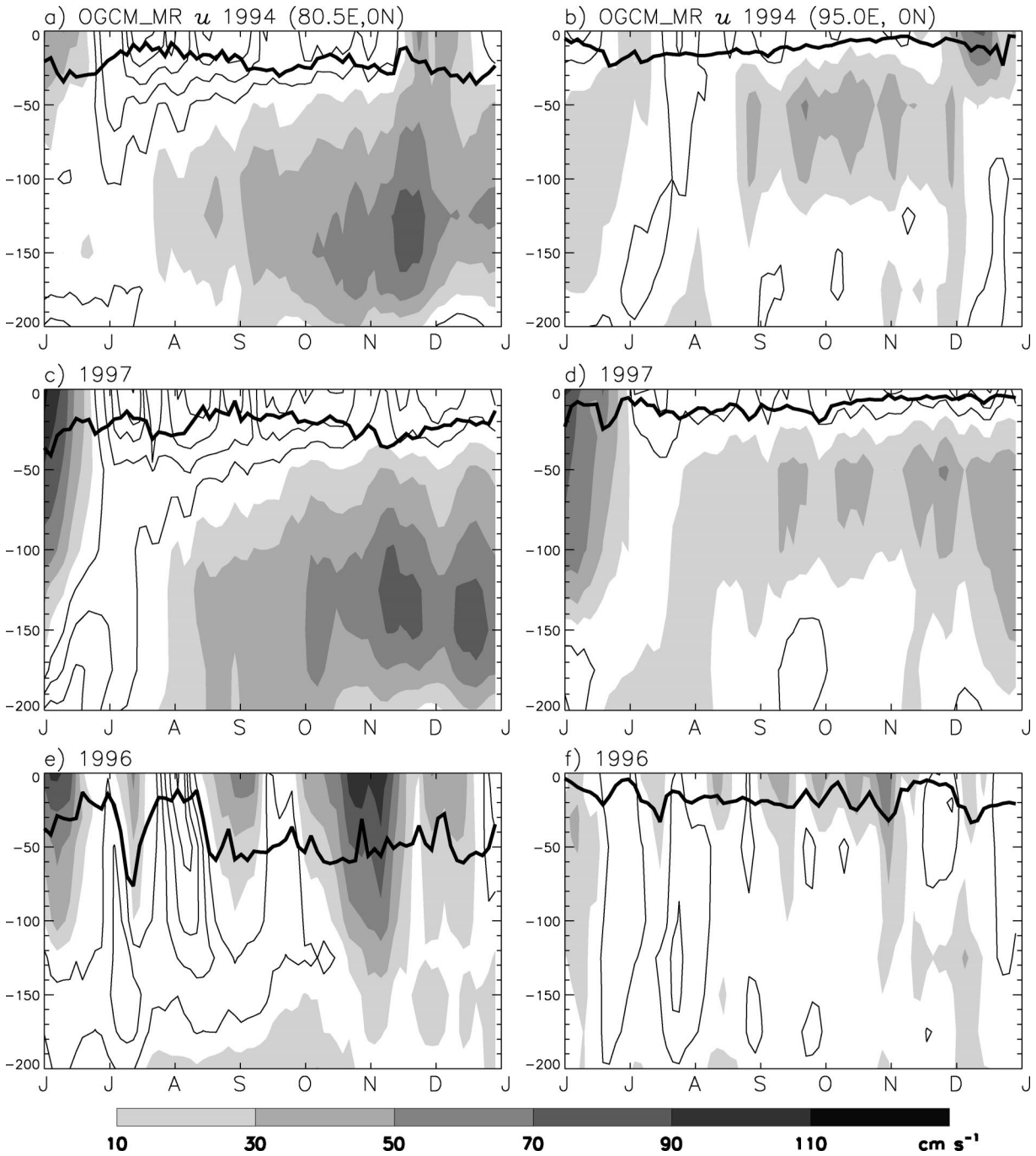

FIG. 15. (a) Time evolution of zonal current, u, on the Indian Ocean equator (0°, 80.5°E) in the upper 200 m from solution OGCM_MR during the 1994 IOZM event; (b) as in (a) but for (0°, 95°E); (c) as in (a) but for 1997 IOZM event; (d) as in (b) but for 1997 IOZM; (e) as in (a) but for 1996; (f) as in (b) but for 1996. Positive values are shaded and negative values are contoured, with an interval of 20 cm s^{-1}. Zero contours are suppressed. The thick solid lines near the surface in the figures show the mixed layer depth from solution OGCM_MR.

4. Summary and conclusions

A thorough investigation is carried out to understand the rectification of intraseasonal atmospheric forcing in zonal surface currents and transport in the equatorial Indian Ocean. A hierarchy of ocean models is used in the tropical Indian Ocean basin: The OGCM–HYCOM is used to provide a realistic estimation for the intraseasonal impact, the linear model is used to demonstrate the nonlinear effect in the OGCM, and the $4\frac{1}{2}$-layer IOM is applied to shed light on the effects of various nonlinear processes that are not easy to isolate in the OGCM.

With the intraseasonal atmospheric forcing, the WJs consist of episodic, swift eastward jets. The westward currents during January–March and during northern summer are composed of strong, episodic westward flow (Fig. 6a). These features are in contrast to the smoothed currents generated by monthly forcing fields that exclude the intraseasonal variability (Fig. 6b). Interestingly, intraseasonal atmospheric forcing not only causes these intraseasonal variations, but it also produces a low-frequency (seasonal to interannual) rectification in current and transport.

A suite of OGCM solutions demonstrates that intraseasonal atmospheric forcing causes westward rectified surface currents during spring and autumn, which weaken the WJs. During January–March and to a lesser degree during summer, the rectified currents are eastward, which weaken the westward surface flow (Fig. 7a). The rectified currents result primarily from intraseasonal winds, and effects due to intraseasonal precipitation and solar shortwave radiation are negligible (Figs. 7a–c). Intuitively, the cross-time-scale impacts likely result from the nonlinearity of the oceanic system, and this is confirmed by the corresponding linear model solution in which the rectified low-frequency currents disappear (Fig. 7d).

Major nonlinear processes that determine the rectified surface currents are an asymmetric response of mixed layer depth to easterly and westerly winds, upwelling, and entrainment of the subsurface water into the surface layer. Horizontal advection plays a minor role.

Easterly winds associated with atmospheric intraseasonal events shoal and westerly winds deepen the surface mixed layer. As a result, a net westward surface current is generated over an event mean since the easterly winds act on a thin surface mixed layer, whereas the westerly winds act on a thicker one. This asymmetric mixed layer response is especially strong during spring and autumn when the seasonal winds are westerlies, accounting for a large part of the WJs weakening [section 3c(1); cf. Figs. 7a and 9b, 12, and 14]. During early spring, when the seasonal winds are easterlies, this effect is small and often has a reversed sign, contributing somewhat to the eastward rectification at this time during some years. This seasonal dependence of mixed layer response to intraseasonal winds reflects the importance of the seasonal background state of winds on oceanic response. During spring and autumn, westerly (easterly) phase of an intraseasonal event increases (decreases or even reverses) the seasonal westerly winds, increases (decreases) entrainment, and therefore thickens (thins) the mixed layer. This entrainment effect reinforces the asymmetric MLD response, producing a significant westward surface flow over an event mean. In contrast, during early spring westerly (easterly) phase of an intraseasonal event tends to decrease (increase) the seasonal easterly winds and entrainment, thinning (thickening) the mixed layer. This entrainment effect counteracts and often dominates the asymmetric MLD response, producing a weak eastward rectified surface flow.

Increased entrainment of the slower subsurface water into the surface mixed layer due to the strong episodic westerlies further weakens the spring and autumn WJs (Figs. 10 and 11). During early spring vertical advection and entrainment of the EUC produce an eastward current rectification, explaining a major part of the rectified low-frequency, eastward surface current at this time of the year (Figs. 11 and 13). This result suggests that the seasonal background state of currents is important in determining the surface current rectification.

While the rectified surface currents are strongly season dependent, strengths of the rectification exhibit a significant interannual variability (Fig. 7a). The seasonality and interannual variability of the rectified surface currents are determined primarily from the seasonal cycle and interannual variability of the background states of winds and currents. Seasonal-to-interannual variability of intraseasonal winds also contribute [sections 3b(2) and 3c(3ii)].

Intraseasonal atmospheric forcing tends to produce a low-frequency, eastward vertically integrated volume and heat transports in the equatorial Indian Ocean with an amplitude of 0–15 Sv for the volume and 0–1.2 PW for the heat [section 3b(3); Figs. 8a,c]. The rectified vertically integrated eastward transport is consistent with the results from earlier studies, which argued that the nonlinear response of the ocean to westerly and easterly winds produces a net eastward transport in the water column [section 3b(3)]. Westerly winds cause equatorial downwelling that advects the surface eastward momentum downward giving subsurface eastward flow. Easterly winds cause equatorial upwelling and generate an eastward pressure gradient force that forces an eastward subsurface current. The subsurface current is advected upward by upwelling. The net effect of the nonlinear response of the ocean over an intraseasonal cycle tends to produce an eastward vertically integrated transport, which results primarily from the layers below the surface mixed layer. Above the thermocline the rectified volume and heat transports are westward during late spring and autumn and eastward during early spring, and to a lesser degree during summer, as the rectified surface currents (Figs. 8b, 8d, and 7a).

The rectified seasonal-to-interannual surface currents and heat transport may affect the advection of SST and the heat storage in the equatorial Indian Ocean warm pool, and thus may exert influence on the warm pool convection.

During the IOZM years (section 3d), easterly wind anomalies drive weak autumn WJs (Fig. 6a) and force EUCs that shoal toward the east (Fig. 15). Rectified surface currents, however, are still westward in the OGCM solution (Fig. 7a), and they result from the dominant effect of the asymmetric MLD response to easterly and westerly winds (Fig. 9). In the IOM solution, the rectified currents are eastward during the same period

of time (Fig. 11), suggesting that vertical advection and entrainment dominate the asymmetric response effect in the IOM. It indicates that the IOM may exaggerate the entrainment and vertical advection processes in comparison with the OGCM. The rectified westward currents during the IOZM events may enhance the westward advection of the colder SSTA. At the mean time, increased entrainment due to intraseasonal wind may contribute some to the rectified cooling effect. Given that the amplitudes of intraseasonal winds appear to be weaker during peaks of the IOZM events, the impact of atmospheric intraseasonal variability on the IOZM may not be large in comparison with their impacts during normal years.

Results from this paper suggest that intraseasonal atmospheric forcing can cause seasonal-to-interannual variability in the coupled tropical ocean–atmosphere system. Therefore, in order to produce accurate seasonal-to-interannual simulations and predictions, high-frequency atmospheric forcing should be taken into account.

Acknowledgments. The authors thank Dr. Alan Wallcraft at the Naval Research Laboratory for his numerous help in configuring the HYCOM to the Indian Ocean domain. We thank NCEP–NCAR and CPC for making the forcing fields available on the Internet, and COAPS of FSU for providing the quality satellite winds on the Internet. Weiqing Han was supported by NSF Grant OCE-0136836, and Peter Webster was supported by NSF ATM-9526030. Peter Hacker and Roger Lukas were supported by NSF Grant ATM-9820531 and NOAA/OGP NA67RJ0154. Aixue Hu was supported by DOE Grant DE-FC03-97ER62402.

REFERENCES

Behera, S. K., R. Krishnan, and T. Yamagata, 1999: Unusual ocean–atmosphere conditions in the tropical Indian Ocean during 1994. *Geophys. Res. Lett.,* **26,** 3001–3004.

Bleck, R., 2002: An oceanic general circulation model framed in hybrid isopycnic-Cartesian coordinates. *Ocean Modell.,* **4,** 55–88.

Bourassa, M. A., M. H. Freilich, D. M. Legler, W. T. Liu, and J. J. O'Brien, 1997: Wind observations from new satellite and research vessels agree. *Eos, Trans. Amer. Geophys. Union,* **78,** 597–602.

Cane, M. A., 1980: On the dynamics of equatorial currents, with application to the Indian Ocean. *Deep-Sea Res.,* **27A,** 525–544.

Duchon, C. E., 1979: Lanczos filter in one and two dimensions. *J. Appl. Meteor.,* **18,** 1016–1022.

Gent, P. R., and M. A. Cane, 1989: A reduced gravity, primitive equation model of the upper equatorial ocean. *J. Climatol.,* **17,** 1513–1534.

Gill, A. E., 1975: Models of equatorial currents. *Proceedings Symposium on Numerical Models of Ocean Circulation,* National Academy of Science, 181–203.

Halliwell, G. R., 1998: Simulation of North Atlantic decadal/multidecadal winter SST anomalies driven by basin-scale atmospheric circulation anomalies. *J. Phys. Oceanogr.,* **28,** 5–21.

——, 2004: Evaluation of vertical coordinate and vertical mixing algorithms in the HYbrid Coordinate Ocean Model (HYCOM). *Ocean Modell.,* **7,** 285–322.

Han, W., 1999: Influence of salinity on dynamics, thermodynamics, and mixed-layer physics in the Indian Ocean. Ph.D. dissertation, Nova Southeastern University, 147 pp.

——, J. P. McCreary, D. L. T. Anderson, and A. J. Mariano, 1999: Dynamics of the eastward surface jets in the equatorial Indian Ocean. *J. Phys. Oceanogr.,* **29,** 2191–2209.

——, D. M. Lawrence, and P. J. Webster, 2001a: Dynamical response of equatorial Indian Ocean to intraseasonal winds: Zonal flow. *Geophys. Res. Lett.,* **28,** 4215–4218.

——, J. P. McCreary, and K. E. Kohler, 2001b: Influence of precipitation–evaporation and Bay of Bengal rivers on dynamics, thermodynamics, and mixed layer physics in the upper Indian Ocean. *J. Geophys. Res.,* **106,** 6895–6916.

Howden, S., and R. Murtugudde, 2001: Effects of river inputs into the Bay of Bengal. *J. Geophys. Res.,* **106,** 19 825–19 843.

Jerlov, N. G., 1976: *Marine Optics.* Elsevier, 231 pp.

Kalnay, E., and Coauthors, 1996: The NCEP/NCAR 40-Year Reanalysis Project. *Bull. Amer. Meteor. Soc.,* **77,** 437–471.

Kessler, W. S., and R. Kleeman, 2000: Rectification of the Madden–Julian oscillation into the ENSO cycle. *J. Climate,* **13,** 3560–3575.

Kraus, E. B., and J. S. Turner, 1967: A one-dimensional model of the seasonal thermocline. II: The general theory and its consequences. *Tellus,* **19,** 98–106.

Large, W. G., J. C. McWilliams, and S. C. Doney, 1994: Oceanic vertical mixing: A review and a model with a nonlocal boundary layer parameterization. *Rev. Geophys.,* **32,** 363–403.

——, G. Danabasoglu, S. C. Doney, and J. C. McWilliams, 1997: Sensitivity to surface forcing and boundary layer mixing in a global ocean model: Annual-mean climatology. *J. Phys. Oceanogr.,* **27,** 2418–2447.

Levitus, S., and T. P. Boyer, 1994: *Temperature.* Vol. 4, *World Ocean Atlas 1994,* NOAA Atlas NESDIS 4, 117 pp.

——, R. Burgett, and T. P. Boyer, 1994: *Salinity.* Vol. 3, *World Ocean Atlas 1994,* NOAA Atlas NESDIS 3, 99 pp.

Masson S., C. Menkes, P. Delecluse, and J. P. Boulanger, 2003: Impacts of salinity on the eastern Indian Ocean during the termination of the fall Wyrtki Jet. *J. Geophys. Res.,* **108**, 3067, doi: 10.1029/2001JC000833.

McCreary, J. P., 1980: Modeling wind-driven ocean circulation. Hawaii Institute of Geophysics Tech. Rep. HIG-80-3, 64 pp.

——, 1981: A linear stratified ocean model of the coastal undercurrent. *Philos. Trans. Roy. Soc. London,* **302A,** 385–413.

——, P. K. Kundu, and R. L. Molinari, 1993: A numerical investigation of dynamics, thermodynamics, and mixed layer processes in the Indian Ocean. *Progress in Oceanography,* Vol. 31, Pergamon, 181–224.

——, W. Han, D. Shankar, and S. R. Shetye, 1996: On the dynamics of the East India Coastal Current. 2: Numerical solutions. *J. Geophys. Res.,* **101** (C6), 13 993–14 010.

McPhaden, M. J., and B. A. Taft, 1988: Dynamics of seasonal and intraseasonal variability in the eastern equatorial Pacific. *J. Phys. Oceanogr.,* **18,** 1713–1732.

Molinari, R. L., D. Olson, and G. Reverdin, 1990: Surface current distributions in the tropical Indian Ocean derived from compilations of surface buoy trajectories. *J. Geophys. Res.,* **95,** 7217–7238.

Murtugudde, R., J. P. McCreary, and A. J. Busalacchi, 2000: Oceanic processes associated with anomalous events in the Indian Ocean with relevance to 1997–1998. *J. Geophys. Res.,* **105** (C2), 3295–3306.

Pedlosky, J., 1987: An inertial theory of the equatorial undercurrent. *J. Phys. Oceanogr.,* **17,** 1978–1985.

Philander, S. G. H., and R. C. Pacanowski, 1980: The generation of equatorial currents. *J. Geophys. Res.,* **85,** 1123–1136.

Reppin, J., F. A. Schott, J. Fischer, and D. Quadfasel, 1999: Equatorial currents and transports in the upper central Indian Ocean: Annual

cycle and interannual variability. *J. Geophys. Res.*, **104,** 15 495–15 514.

Robinson, A. R., 1966: An investigation into the wind as the cause of the equatorial undercurrent. *J. Mar. Res.*, **24,** 170–204.

Saji, N. H., B. N. Goswami, P. N. Vinayachandran, and T. Yamagata, 1999: A dipole mode in the tropical Indian Ocean. *Nature*, **401,** 360–363.

Senan, R., D. Sengupta, and B. N. Goswami, 2003: Intraseasonal monsoon jets in the equatorial Indian Ocean. *Geophys. Res. Lett.*, **30**, 1750, doi:10.1029/2003GL017583.

Shankar, D., J. P. McCreary, W. Han, and S. R. Shetye, 1996: On the dynamics of the East India Coastal Current, Part 1: Analytic solutions forced by interior Ekman pumping and local alongshore winds. *J. Geophys. Res.*, **101** (C6), 13 975–13 991.

Shinoda, T., and H. H. Hendon, 2002: Rectified wind forcing and latent heat flux produced by the Madden–Julian oscillation. *J. Climate*, **15,** 3500–3508.

Vinayachandran, P. N., S. Iizuka, and T. Yamagata, 2002: Indian Ocean dipole mode events in an ocean general circulation model. *Deep-Sea Res.*, **49B,** 1573–1596.

Waliser, D. E., R. Murtugudde, and L. E. Lucas, 2003: Indo-Pacific Ocean response to atmospheric intraseasonal variability: 1. Austral summer and the Madden–Julian Oscillation. *J. Geophys. Res.*, **108,** 3160, doi:10.1029/2002JC001620.

Webster, P. J., A. M. Moore, J. P. Loschnigg, and R. R. Leben, 1999: Coupled ocean–atmosphere dynamics in the Indian Ocean during 1997–1998. *Lett. Nature*, **401,** 356–360.

——, and Coauthors, 2002: The JASMINE pilot study. *Bull. Amer. Meteor. Soc.*, **83,** 1603–1630.

Wyrtki, K., 1973: An equatorial jet in the Indian Ocean. *Science*, **181,** 262–264.

Xie, P., and P. A. Arkin, 1996: Analyses of global monthly precipitation using gauge observations, satellite estimates, and numerical model predictions. *J. Climate*, **9,** 840–858.